Nanoscale

REVIEW

View Article Online
View Journal | View Issue

Cite this: *Nanoscale*, 2026, **18**, 7825

Nanostructured high-entropy oxides for catalysis: linking entropy to function

Zhuxin Lyu,†[a] Yunpeng Wang,†[a,b] Yueming Sun[a] and Yunqian Dai *[a]

High entropy oxides (HEOs) are gaining rapid attention due to densely distributed active centers, tunable surface areas, robust lattices, flexible geometries and self-balanced electronic states. These features give them activity and durability that single- or binary-metal oxides rarely match in thermal, electro- and photocatalysis. We systematically examine four entropy-driven effects, namely high-entropy stabilization, severe lattice distortion, sluggish diffusion and cocktail-like multi-element synergy, all of which govern phase formation, defect chemistry and functional performance. By simultaneously optimizing the surface area, lattice robustness and scalable processing, we outline how porous architectures, low-temperature integrity, phase control and high-throughput manufacturing are merged into a single framework. Complex disordered structures of HEOs challenge traditional characterization, demanding advanced methods. *In situ* vibrational spectroscopy, *operando* X-ray characterization, DFT and artificial-intelligence converge to resolve the dynamic structure–property relationships that underpin HEO catalysis. We hope this review sparks wider interest in high-entropy oxides and accelerates their path from laboratory curiosity to industrial catalysts.

Received 16th December 2025,
Accepted 20th February 2026

DOI: 10.1039/d5nr05294g

rsc.li/nanoscale

1. Introduction

From the Stone Age to the Industrial Revolution, materials mastered by humankind have repeatedly defined the limits of civilizations.[1] As the global energy system shifts from fossil fuels to renewables, and as device performance approaches intrinsic physical limits, established materials are reaching their performance ceilings faster than ever before. Identifying materials that can overcome these limitations is now the top priority in contemporary materials science. On this background, the high-entropy paradigm emerged. In 2004, high-entropy alloys revealed that entropic stabilization could unlock vast, previously inaccessible compositional spaces, ushering in a whole new approach to alloy

[a]*School of Chemistry and Chemical Engineering, Southeast University, Nanjing, Jiangsu 211189, P. R. China. E-mail: daiy@seu.edu.cn*
[b]*School of Materials Science and Engineering, Hebei University of Science and Technology, Shijiazhuang, Hebei 050018, P. R. China*
†These authors contributed equally to this work.

Zhuxin Lyu

Zhuxin Lyu completed her undergraduate studies in Chemical Engineering and Technology at the School of Chemical and Materials Engineering, Jiangnan University (Sep. 2019–Jun 2023). During this period, she mainly worked on surfactant-related research and finished her graduation thesis. Since Sep. 2024, she has been a master's student in Chemical Engineering at the School of Chemistry and Chemical Engineering, Southeast University. Her current research focuses on the design of nanofiber materials, performance regulation, and their applications in thermal catalysis.

Yunpeng Wang

Yunpeng Wang is a Lecturer in the School of Materials Science and Engineering at Hebei University of Science and Technology. He received his Ph. D. from the School of Chemistry and Chemical Engineering, Southeast University in 2025, and subsequently joined the faculty at Hebei University of Science and Technology. His research focuses on the design and development of nanofibers and anti-sintering catalysts for energy and environmental applications.

design.[2] This concept was confined to metals until 2015, when the first single-phase high-entropy oxide (HEO) was demonstrated to show that entropy-driven homogenization is equally powerful in ionic lattices.[3] This proof of concept sparked a surge of interest, and within a decade, HEOs had spread across various structural families, including rock-salt, spinels, perovskites and fluorites. They have already demonstrated record-breaking performance in catalysis, energy storage, dielectrics and solid-state ionics.[4,5] For instance, high-entropy spinel oxide $Sn_{0.8}$(Co,Mg,Mn,Ni, $Zn)_{2.2}O_4$ fundamentally suppresses volume expansion during lithiation by forming a homogeneous amorphous multicomponent matrix, enabling the Li-ion battery anode to maintain nearly 100% capacity after 500 cycles.[6]

The high-entropy concept opens a broad design space for functional oxides. By mixing five or more cations on one sub-lattice, HEOs can stabilize disordered lattices, widen processing windows, and introduce local strain, charge imbalance, and bonding heterogeneity that are difficult to realize in conventional solids.[7–9] These features yield greater thermal robustness, slower ionic inter-diffusion and emergent electronic or catalytic properties that surpass the sum of the parts.[10–12] Yet most studies remain empirical or focus on isolated cases; what is still missing is a unified framework that ties high entropy, severe lattice distortion, sluggish diffusion and cocktail-like multi-element cooperativity to measurable performance gains and explains how they act in concert to control structure formation, stability and property emergence.[13,14] Establishing a unified framework linking entropy, structure, and catalytic function will accelerate rational design and industrial deployment of high-entropy oxides from laboratory to catalysis and energy technologies.

Anchored in the synergy among configurational entropy, structural disorder, and functional performance, this review establishes an entropy–structure–function paradigm that elucidates how thermodynamic design principles govern the genesis of catalytic properties in high-entropy oxides. Specifically, configurational entropy serves as a tunable thermodynamic variable that expands accessible compositional spaces and entropy-stabilizes single-phase oxides against phase separation, thereby enabling systematic tuning of multication compositions. This entropic stabilization generates structural complexity transcending the average crystal lattice to encompass local coordination environments, strain fields, and oxygen-sublattice distortions, which collectively govern defect formation and redox adaptability, ultimately translating compositional disorder into catalytic function through diverse adsorption strengths and cooperative multi-site reaction pathways. Building upon this foundation, we demonstrate how the high-entropy effect, lattice distortion effect, sluggish diffusion effect, and cocktail effect collectively dictate phase stability and property genesis, consolidating quantitative definitions and structural families of HEOs. We subsequently review advances in synthesis spanning low-temperature and high-surface-area routes, which lock in single-phase compositions while preserving active architectures. Furthermore, we integrate advanced *in situ*/*operando* probes, multiscale simulations and machine-learning workflows to decode dynamic structure–property relationships under realistic operating conditions. Finally, these insights are distilled into comprehensive design guidelines covering element selection, synthesis methods, mechanistic investigations, advanced characterization techniques, theoretical considerations, and scalable processing, offering a concise roadmap for translating high-entropy oxides from laboratory curiosities into scalable technologies for energy and environmental applications.

Yueming Sun

Yueming Sun received a PhD degree in coordination chemistry from Nanjing University in 1991. He is a professor in the School of Chemistry and Chemical Engineering at Southeast University. His research interests include dye molecular engineering, theoretical and computational chemistry, and design and synthesis of novel nano-electrodes and electrolytes for applications in solar cells, batteries, and fuel cells.

Yunqian Dai

Yunqian Dai received her Ph.D. in Materials Physics and Chemistry from Southeast University in 2011. She spent two years as a visiting graduate student at Washington University in St. Louis from 2008 to 2010. She started as an Assistant Professor in the School of Chemistry and Chemical Engineering in Southeast University in 2011 and was then promoted to Professor in 2019. Her current research interests include electrospun nano fibers and their applications in catalysis, environmental science, and energy conversion.

2. Definition, structural characteristics, and fundamental properties

High-entropy oxides derive from the broader concept of high-entropy materials. Configurational entropy is deliberately maximized here to stabilize simple solid solutions in which multiple principal elements share a common lattice. The original framework was established in metallic high-entropy alloys. Equiatomic or near-equiatomic mixing of several metals forms single-phase solid solutions instead of complex intermetallic mixtures.[15] This concept has been extended to ceramics. Multiple cations occupy one or more crystallographic sublattices in ceramics to form high-entropy ceramics, including nitrides, carbides, borides, and oxides.[16] Among these materials, high-entropy oxides are a particularly versatile class of functional materials. They possess tunable electronic, ionic, magnetic and dielectric properties that originate from strong coupling between disorder, local chemistry and lattice dynamics.[17]

2.1 Definition of entropy

Entropy, as a core concept in thermodynamics, was initially defined by Boltzmann's formula and is used to describe the disorder of a system or the number of microscopic states.

$$S = k_B \ln W \quad (2-1)$$

Here, k_B represents the Boltzmann constant and W denotes the number of microscopic states of the system. Conformational entropy describes the diversity of arrangements of different components at equivalent lattice sites. The calculation formula for the configurational entropy of an oxide is

$$S = -R\left[\left(\sum_{i=1}^{N} x_i \ln x_i\right)_{\text{cation-site}} + \left(\sum_{j=1}^{N} x_j \ln x_j\right)_{\text{anion-site}}\right]. \quad (2-2)$$

Here, R represents the ideal gas constant, and x_i and x_j respectively denote the mole fraction of the x-th component (where $x = i$ or j) at the cation sites and anion sites. It can be inferred that when the mole fractions of each component are equal, the value of ΔS_{mix} will reach its maximum. As the number of components in the material system increases, the configurational entropy significantly rises. Based on this principle, researchers proposed the concept of high entropy, namely that when multiple metal elements coexist in nearly equal molar ratios, their high configurational entropy can effectively stabilize the solid-solution structure.[18] Therefore, high-entropy oxides are defined as: an oxide system of solid solutions composed of five or more metal elements in an equimolar or nearly equimolar ratio. The phase stability of such oxides mainly depends on the high configurational entropy effect.

High-entropy oxides therefore represent a design space in which configurational entropy is treated as an explicit materials design parameter rather than a secondary effect. Studies on high-entropy ceramics and high-entropy oxides have emphasized that rational design requires simultaneous consideration of thermodynamic stability, mixing behavior on different sublattices, and kinetic constraints during synthesis.[16,19] This perspective has motivated the development of phase stability maps, descriptor-based screening, and data-driven approaches that couple entropy with enthalpy, electronic structure, and defect chemistry.

2.2 Structural types of high-entropy oxides

High-entropy oxides can exhibit a variety of crystal structures, in which oxygen anions form a relatively simple sublattice, while multiple cations share one or more crystallographic sites within the unit cell, with near-random occupancy of these sites. In addition to more complex structures, the most widely studied structural families include rock-salt, fluorite, perovskite, and spinel lattices.[20]

In rock-salt-type high-entropy oxides (*e.g.*, (MgCoNiCuZn)O), oxygen ions form a face-centered cubic sublattice, while divalent cations occupy octahedral sites (Fig. 1a).[3] The random distribution of cations creates a chemically disordered yet topologically simple lattice, where the local environments of individual sites exhibit significant variations, yet long-range cubic symmetry is preserved. These materials have emerged as model systems for studying the formation of entropy-stabilized phases and also serve as functional materials with tunable electrical properties and defect chemistry characteristics. Systematic investigations of the electrical transport properties of rock-salt-type high-entropy oxides and their doped derivatives reveal the coexistence of hopping conduction and polaron conduction. The conductivity and activation energy of these materials can be modulated through cation selection and heterovalent substitution.[21]

The general formula of fluorite-type high-entropy oxides is typically $AO_{2-\delta}$, where A represents a mixture of tetravalent or mixed-valence cations, including rare-earth or transition-metal ions such as zirconium, hafnium, and cerium (Fig. 1b). In this structure, the cations are arranged in a face-centered cubic lattice, while oxygen ions occupy tetrahedral interstitial sites, with each cation having a coordination number of eight. Charge compensation is usually achieved through randomly distributed oxygen vacancies, the presence of which significantly influences ionic transport properties and thermal characteristics. Reported single-phase fluorite-type high-entropy oxides (*e.g.*, $Zr_{0.2}Hf_{0.2}Ce_{0.2}Sn_{0.2}Mn_{0.2}O_{2-\delta}$) exhibit extremely low thermal conductivity, moderate bandgaps, and excellent high-temperature structural stability.[22] The combination of cation lattice disorder and mobile oxygen defects not only induces strong phonon scattering effects but also maintains the integrity of the fluorite structure. These materials hold great promise for thermal barrier coatings and multifunctional applications requiring tailored thermal transport properties.[23]

Perovskite high-entropy oxides extend the classical ABO_3 framework to multi-principal cation compositions on the A

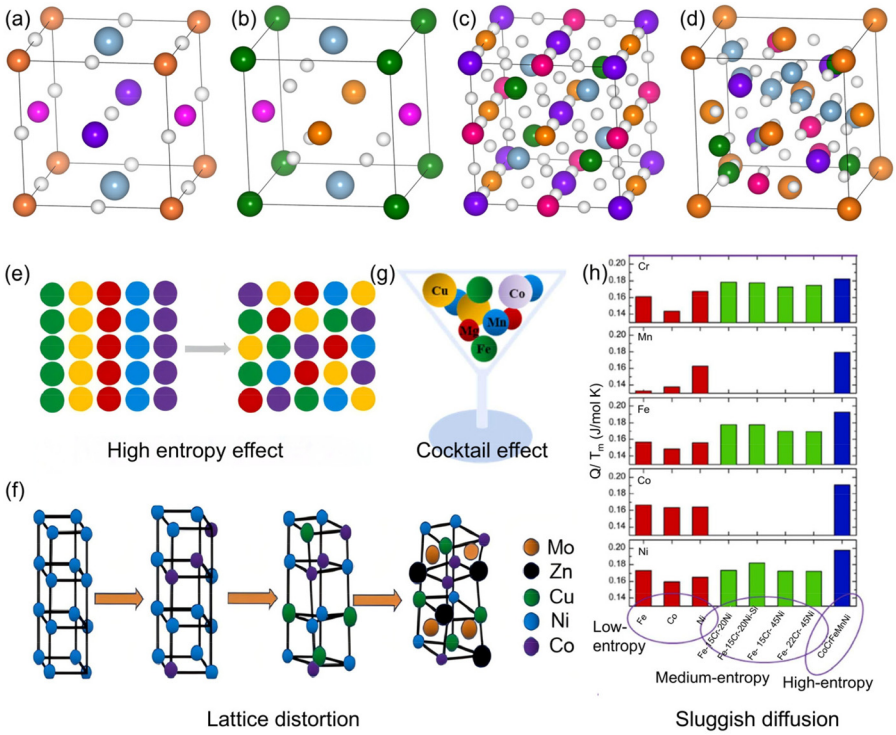

Fig. 1 Structural types and four core effects in high-entropy oxides. Common crystal structures: (a) rock-salt, (b) fluorite, (c) perovskite, and (d) spinel structures. Four core effects: (e) high entropy effect, (f) lattice distortion, (g) cocktail effect, and (h) sluggish diffusion. Copyright 2022, Elsevier.[46]

site, the B site, or both (Fig. 1c). In many high-entropy perovskites, rare-earth and alkaline-earth ions share the A sublattice, whereas several transition metals occupy the B sublattice, which introduces extensive local distortions of the octahedra.[24] Studies on high-entropy perovskite cathodes for solid oxide fuel cells have demonstrated that compositions with multiple A-site and B-site cations can still maintain a single perovskite phase with well-defined oxygen octahedra and controllable oxygen non-stoichiometry.[25] The disordered cation distribution modifies the bonding environment and regulates the concentration and mobility of oxygen vacancies, which in turn governs electronic conductivity and surface exchange kinetics.

Spinel-type high-entropy oxides typically follow the general formula AB_2O_4, featuring a cubic crystal structure with the space group $Fd\bar{3}m$ (Fig. 1d). In this structure, oxygen atoms form a face-centered cubic (fcc) close-packed framework, while A-site ions predominantly occupy tetrahedral interstitial positions and B-site ions reside in octahedral sites under ideal conditions. Both A and B sites exhibit excellent multi-element accommodation, offering greater degrees of freedom for composition design and property modulation than rock-salt or fluorite-type high-entropy oxides. Existing studies have successfully synthesized single-phase spinel high-entropy oxides such as $(Mn_{0.2}Fe_{0.2}Ni_{0.2}Mg_{0.2}Zn_{0.2})_3O_4$, with characterization confirming uniform elemental distribution across the cation sublattices.[26] The spinel topology endows A and B sites with rich redox activity and constructs interconnected diffusion channels, which facilitate the transport of both cations and anions. Electrochemical investigations on spinel high-entropy oxides (*e.g.*, $(Mg_{0.2}Ti_{0.2}Zn_{0.2}Cu_{0.2}Fe_{0.2})_3O_4$) for lithium-ion battery applications, particularly as anode materials, have demonstrated that the multi-cation environment significantly accelerates reaction kinetics and enhances cycling stability. Moreover, the underlying spinel framework maintains structural integrity during repeated lithium insertion–extraction and phase transition processes.[27]

These four structure types provide a common structural basis for most high-entropy oxides reported so far. Rock-salt and fluorite lattices offer simple cation environments and high symmetry, which are advantageous for disentangling the effects of entropic stabilization and lattice distortion. Perovskite and spinel structures introduce multiple crystallographic sites, enabling more complex couplings between charge, spin, orbital, and defect degrees of freedom. Understanding how configurational disorder interacts with each of these structure families is essential for rational design of functional properties and for expanding high-entropy concepts to more complex oxide chemistries.[28]

2.3 Key entropy-driven effects in high-entropy oxides

High-entropy oxides, due to their unique structural disorder, element diversity and designability of properties, have demonstrated four core effects, making them an important research direction in the field of new functional materials. These effects

interact with each other at the thermodynamic, structural, dynamic and functional levels, jointly endowing the materials with breakthrough comprehensive properties.[29]

2.3.1 High entropy effect. The high-entropy effect refers to the phenomenon where the configurational entropy generated by the random mixing of multiple cations stabilizes a single solid-solution phase (Fig. 1e). In high-entropy oxides, when five or more metals occupy the same crystallographic sites in near-equimolar proportions, the mixing entropy (ΔS_{mix}) increases significantly (typically $\Delta S_{mix} > 1.5R$, where R is the gas constant), thereby substantially reducing the Gibbs free energy (ΔG_{mix}) of the system. This mechanism enables simple crystal structures such as rock salt, fluorite, perovskite, and spinel structures to maintain a single-phase state within composition ranges where traditional phase diagrams predict multiphase coexistence.[30]

Thermodynamically guided synthesis strategies have now made it possible to more precisely quantify the high-entropy effect. Heating can promote the formation of disordered solid solutions, while suppressing ion diffusion during cooling can preserve this disordered state. A recent thermodynamically inspired design study confirmed that by balancing the enthalpy interactions and configurational entropy of the system, it is possible to effectively predict whether a specific cation combination will form a single-phase high-entropy oxide or undergo phase separation. This provides a more predictive theoretical foundation for the compositional design of high-entropy oxides.[31]

2.3.2 Lattice distortion. Lattice distortion refers to the static and dynamic deviations of local bond lengths and angles relative to the average crystal structure (Fig. 1f). It originates from atomic-scale local environmental mismatches. In traditional doping systems, the introduction of heteroatoms only leads to micron-scale lattice adjustments. In high-entropy oxides, due to the often more pronounced differences in cation sizes and bonding modes, the lattice distortion effect is more prominent. In ideal high-entropy materials, the random distribution of elements ensures that each atom is surrounded by different heteroatoms, and the inherent property differences among these atoms inevitably cause displacements of lattice sites. This "distortion" helps release the system's internal energy, thereby achieving thermodynamic stability of the material.[32] Recent studies on lattice distortion in high-entropy oxides confirm that the resulting strain fields lead to diffraction peak broadening, alter local coordination environments, and induce strong phonon scattering.[33]

Experimental and atomic simulation results from rare-earth high-entropy silicate model systems demonstrate that, compared to single-component reference materials, high-entropy compositions exhibit significant strain effects and fluctuations in bond strength at the atomic scale. These structural deformations reduce the material's lattice thermal conductivity and modulate its thermophysical properties over a wide temperature range.[34] Similar phenomena have been observed in other high-entropy ceramics: the synergistic effects of structural deformation and mass fluctuations can lower thermal conductivity while maintaining phase stability. This characteristic holds significant importance for applications in thermal barrier coatings and thermoelectric fields.[35]

2.3.3 Cocktail effect. The cocktail effect refers to the emergence of unique properties that cannot be predicted by simple mixing rules when multiple elements interact synergistically (Fig. 1g). High-entropy materials, composed of diverse elements with distinct characteristics, exhibit complex and specialized performance due to their multifaceted interactions. In high-entropy oxides, this effect often manifests as simultaneous improvements in multiple performance metrics or significant nonlinear trends closely tied to composition.[36] A recent study on eggshell-like high-entropy oxide catalysts demonstrated that introducing five or more cations into a mesoporous oxide framework resulted in superior catalytic activity and stability compared to their single-component oxide counterparts. The authors attributed this advantage to the unique synergistic electronic and structural effects inherent to multicomponent combinations.[37]

Similar phenomena also exist in high-entropy calcium titanate oxides. A multi-site calcium titanate $La_{0.5}Sr_{0.5}Mn_{0.15}Fe_{0.15}Co_{0.4}Ni_{0.15}Cu_{0.15}O_3$ electrocatalyst, achieved by B-site co-doping with multiple transition metals, delivers markedly improved oxygen evolution reaction performance, requiring an overpotential of only 309 mV at 10 $mA{\cdot}cm^{-2}$, which is lower than the low entropy oxide (396 mV).[38] Analysis of the local structure and electronic states confirmed that the mixed B-site environment constructed abundant adsorption sites and reaction pathways, which is the core feature of the "cocktail effect". Extensive research on high-entropy energy materials further indicates that this kind of synergistic effect is also manifested in dielectric responses, thermoelectric performance, and electrochemical cycling. The complexity of composition enables the materials to possess characteristics such as low thermal conductivity, excellent electrical conductivity, and chemical stability, which are often difficult to achieve simultaneously in traditional oxides and are of great significance for the development of related functional materials.[39]

2.3.4 Sluggish diffusion effect. The sluggish diffusion behavior originated from the study of high-entropy alloys, where the interplay of diverse local atomic environments and migration barriers leads to a significant reduction in diffusion rates (Fig. 1h). Early studies on interfacial diffusion in face-centered cubic high-entropy alloys confirmed that, at comparable homologous temperatures, the diffusion rates in multicomponent systems are markedly lower than those in simple metals.[40] Subsequent research refined this understanding, revealing that the diffusion behavior in high-entropy alloys depends on composition and temperature, and the phenomenon of reduced diffusion rates is not universally observed.[41]

In high-entropy oxides, the concept of sluggish diffusion has two primary applications. On the one hand, slow cation diffusion helps maintain a single-phase solid-solution structure during cooling and operation, thereby preserving entropy-stabilized phases and inhibiting grain growth. On the other

hand, it facilitates controlled diffusion in solid electrolytes and battery materials, where one species (*e.g.*, Li^+ or O^{2-}) must be mobile while the framework cations remain immobile. A recent study demonstrated that a multi-cation framework can create a kinetically stable host lattice while enabling rapid ion transport through a carefully designed defect network.[11] Additionally, research on diffusion behavior across a wide compositional range of high-entropy oxides suggests that diffusion properties are better described by a distribution of migration energy barriers rather than a single activation energy, reflecting the complexity of local environments in these materials.[42]

Rather than acting in isolation, these four high-entropy effects cooperate (Table 1). The high-entropy effect arises from large configurational disorder. This disorder intensifies local lattice distortion as atoms of different sizes and electronic characters occupy the same lattice. The resulting distortion not only helps stabilize single-phase structures but also alters local bond strengths and electronic states.[33] The distorted lattice creates a complex landscape of migration for atomic motion. In such a landscape, certain migration pathways have higher energy barriers while other pathways act as traps, slowing down net diffusion rates and reinforcing the sluggish diffusion effect.[43] At the same time, the cocktail effect emerges from cooperative interactions among multiple elements. This synergy is modulated by both the degree of lattice distortion and the distribution of mobile species in the distorted lattice.[44]

The roles of the four effects can be summarized as an entropy–structure–function map, where each effect is linked to a core structural descriptor, common experimental readouts, and representative catalytic outcomes (Table 1). Their concerted action flattens the free-energy landscape and frustrates phase separation. A quantitative example is provided by a high-entropy spinel $(CoFeNiMnW)_3O_4$, which delivers an OER overpotential of 256 mV at 10 mA cm^{-2} and maintains >200 h operation at an industrial current density of 500 mA cm^{-2} in alkaline media, while $(CoFeNi)_3O_4$ and Co_3O_4 display obvious degradation, with overpotentials increasing by 110 and 58 mV over 200 h.[45] In a word, HEOs outperform their low- and medium-entropy counterparts in catalytic performance and thermal stability, turning compositional disorder into a systematic performance advantage.

3. Synthesis strategies of HEO nanomaterials

Fundamentally governing the defect landscape and ultimately the catalytic properties of HEOs is their synthesis process. Unlike conventional single or binary oxides, these multicomponent systems require rigorous control of cation distribution, phase stability, and microstructure to fully harness configurational entropy rather than succumb to phase segregation. Synthetic strategies have advanced beyond simple high-temperature solid-state routes to more sophisticated approaches guided by entropy and morphology in recent years. These approaches concurrently take into account surface area, lattice stability, and process scalability. Importantly, these strategies are intrinsically connected. Low-temperature routes mainly lock in composition and oxidation states at the atomic level. Phase control selects and stabilizes the target lattice and its defect chemistry at the crystal level. Porous architectures translate these structural advantages into accessible interfaces at the nanoscale. High-throughput manufacturing then screens compositions and processing windows efficiently and accelerates transfer into films, electrodes, and devices. Together, they form a synergistic workflow that spans from atomic mixing to device-level implementation. The subsequent subsections will address, in turn, high surface area and porous architectures, low-temperature synthesis for compositional integrity, phase modulation and structural retention, and high-throughput, scalable manufacturing, thereby establishing a coherent framework for HEO design spanning from the atomic scale to the device level.

3.1 High-surface-area and porous architectures

High-entropy oxides are intrinsically prone to grain coarsening and pore collapse during high-temperature synthesis, making the deliberate design of high-surface-area and porous architec-

Table 1 Entropy–structure–function map for HEOs

Entropy-driven effect	Core descriptor	Interaction	Experimental readouts	Representative catalytic outcome
High entropy effect	Phase stabilization	Amplifies lattice distortion; provides base disorder	XRD (phase purity); STEM-EDS (homogeneity); *operando* XRD/XAS (phase retention)	Stable activity after aging; suppressed phase separation
Lattice distortion	Local coordination dispersion	Reinforces the sluggish diffusion effect; tunes synergy	EXAFS; IR	Broadened adsorption-strength distribution; improved redox flexibility
Cocktail effect	Non-linear synergy	Enabled by distortion and distribution of sites	Composition libraries; high-throughput screening maps	Performance beyond linear mixing; co-optimization of activity and stability
Sluggish diffusion	Slowed sintering	Results from distortion; impacts species redistribution	Thermal aging and microscopy; diffusion tests;	Enhanced durability; slower deactivation; stable performance

tures a central synthetic challenge. A synthetic method based on electrospinning indicates that a series of multi-metal precursors and polymers can be transformed into high-entropy oxide nanofibers with diverse compositions, with diameters of approximately 50–100 nm, a specific surface area close to 200 $m^2 \cdot g^{-1}$, and well-defined single-phase spinel, perovskite, and cubic lattice structures.[47] In that work, careful matching of the coordination chemistry of the metal precursors and control over sol–gel kinetics during electrospinning enabled homogeneous mixing of multiple cations at the molecular level, allowing crystallization at relatively low temperatures to lock in both the entropy-stabilized phase and the nanofibrous morphology (Fig. 2a).

In addition to simply increasing the surface area, porous high-entropy oxide nanofibers can also act as dynamic supports, using configurational entropy to regulate easily sinterable nanoparticles under harsh conditions. In another paper that reported the synthesis of porous spinel-type high-entropy oxide nanofibers using electrospinning (Fig. 2b), the nanofibers were used as a carrier for ultrafine platinum.[48] After severe thermal aging at 900 °C and subsequent treatment at 500 °C, entropy-driven platinum would re-disperse from aggregated lumps back to a smaller nanoparticle state, almost restoring the original CO oxidation activity. The high-entropy oxide nanofibers prepared using electrospinning technology were also used as catalysts with high surface area for the selective oxidation of volatile organic compounds. Optimizing spinning parameters and calcination conditions can yield a robust mesoporous network with uniformly distributed multielement active sites and improve the conversion rate and stability. These results collectively indicate that the high surface area and porous structure in fibrous high-entropy oxides not only provide more active sites but also enable entropy-driven metal–support interactions, which are difficult to achieve in traditional single-metal oxides.

In addition, high-entropy oxide powders and films with a high surface area and porous structure can be prepared by mechanical chemical methods and sol–gel methods. First, various metal precursors are subjected to high-energy ball milling (Fig. 2c), followed by calcination at a relatively low temperature to obtain the HE-$MgAl_2O_4$ catalyst with a BET surface area of approximately 139 $m^2 \cdot g^{-1}$. Its mesopore size

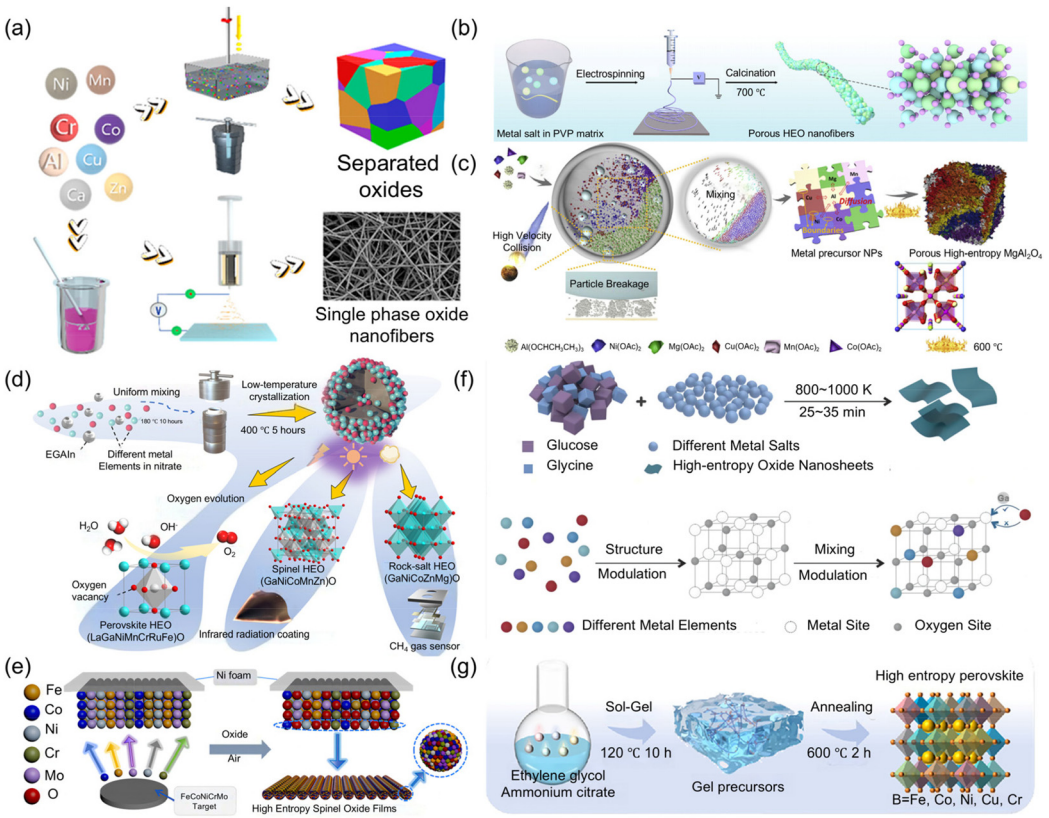

Fig. 2 Synthesis strategies of HEOs. (a) Electrospinning route to high-surface-area single-phase spinel, perovskite, and rock-salt HEO nanofibers. Copyright 2024, American Chemical Society.[47] (b) Porous high-entropy oxide nanofibers prepared by electrospinning. Copyright 2025, Wiley-VCH.[48] (c) Mechanochemical synthesis of porous HE-$MgAl_2O_4$-type spinels. Copyright 2021, Elsevier.[49] (d) Liquid-metal-assisted low-temperature hydrothermal synthesis of Ga-based high-entropy oxides. Copyright 2025, American Association for the Advancement of Science.[53] (e) Magnetron sputtering for high-entropy spinel oxide thin films. Copyright 2025, Science Press.[54] (f) The synthesis of ultrathin high-entropy oxides guided by a self-lattice framework, and with a controllable phase state. Copyright 2024, American Chemical Society.[61] (g) Crystal-phase modulation of high-entropy perovskite oxides. Copyright 2025, Wiley-VCH.[62]

distribution is narrow, and it exhibits excellent stability when oxidizing methane in a hot and humid feed, highlighting the ability of configurational entropy to stabilize crystal structures and mesopore frameworks.[49] The sol–gel strategy can generate spherical mesoporous high-entropy oxides with surface areas ranging from 42 to 143 $m^2 \cdot g^{-1}$ and pore diameters of 5.5 to 8.3 nm. The polymerizable ligands and block copolymer templates define a spinel framework that remains porous even after crystallization.[50]

3.2 Low-temperature synthesis for compositional integrity

Reducing the synthesis temperature is crucial for retaining volatile or oxidation–reduction-sensitive cations and stabilizing the metastable high-entropy structures that may decompose or separate under harsh calcination conditions. Conventional ceramic solid-state routes typically involve prolonged powder mixing and multiple high-temperature calcination steps to achieve chemical homogeneity and phase purity, which becomes increasingly time- and energy-intensive as the compositional complexity increases. In contrast, low-temperature wet-chemical or combustion-derived precursor routes can shorten diffusion distances and reduce the thermal budget, thereby improving compositional retention for volatility- and redox-sensitive cations.[51,52] Increasingly, studies have shown that by designing the reaction medium and thermodynamic driving forces, single-phase multi-cation oxides can be obtained at lower temperatures without sacrificing the uniformity of the composition, which is particularly important for high-entropy oxides whose functions are highly sensitive to the oxidation state and local coordination environment.[7]

By introducing gallium as the reaction medium, gallium-based high-entropy oxides with tunable properties can be synthesized under low-temperature conditions.[53] In this method, first, the multi-metal precursors are assembled onto the liquid gallium through the hydrothermal method, and then after calcination at a temperature of only 400 °C (Fig. 2d), single-phase gallium-based high-entropy oxides with rock salt, spinel or perovskite structures can be obtained, depending on the adjustment of the ionic radius and valence. The negative mixing enthalpy between gallium and transition metal species reduces the overall Gibbs free energy of the mixture, and together with the inherent dynamic liquid metal environment, promotes uniform cation distribution and inhibits separation phenomena even below the traditional entropy-stable temperature.

Magnetron sputtering technology is a low-temperature vapor-phase synthesis method that can produce high-entropy oxide films with uniform composition, uniform coverage, and a nano-scale grain structure. By sputtering high-entropy alloy target materials onto nickel foam at a low substrate temperature with argon as the protective gas, a uniform multielement layer is formed. This layer spontaneously oxidizes in the air to form a single-phase spinel film ($(FeCoNiCrMo)_3O_4$) (Fig. 2e), with the average size of its nano-crystals approaching 2.5 nm.[54] The resulting film has an oxygen evolution overpotential of approximately 216 millivolts at a current of 10 microamperes per square centimeter, and can maintain stability for over 200 hours at a current of 100 microamperes per square centimeter. This indicates that the low-temperature sputtering oxidation process can lock in an unstable multi-ion structure while generating a large number of grain boundaries and defect sites. Due to the relatively mild substrate temperature and subsequent treatment, the volatile-driven component drift is minimized, and the cation distribution is mainly controlled by the sputtering jet rather than by high-temperature diffusion, which is beneficial for precisely designed high-entropy compositions.

In addition, the researchers employed a solvothermal–annealing strategy to prepare single-phase spinel high-entropy oxides $(Co, Cu, Fe, Mn, Ni)_3O_4$ with an average particle size of approximately 5 nanometers. The synthesis temperature was much lower than that of traditional ceramic processing, and it exhibited excellent activity for water decomposition.[55] Due to the enhanced transport and nucleation dynamics of supercritical water, high-entropy spinel nanoparticles with uniform cation mixing and OER activity can be directly generated through supercritical hydrothermal treatment.[56] Moreover, this concept of continuous supercritical hydrothermal flow has been extended to continuous flow reactors. In these reactors, this process allows HEO to form at relatively low temperatures within a timescale of seconds. The synthesized perovskite-type HEO natural gas molecules contain 10 metal elements, indicating that by carefully controlling the hydrothermal conditions, extremely complex components can be stabilized without the need for high-temperature sintering methods.[57]

Taken together, liquid-metal, vapor-phase, and hydrothermal low-temperature methods clarify several core principles for the design of high-entropy oxides. Mixed enthalpy, configurational entropy, and reaction environment must be engineered in a coordinated manner. The thermodynamic driving forces for phase separation and component volatility should be weakened, while the contribution of configurational entropy must remain sufficient to stabilize a single high-entropy phase. When this balance is reached, high-entropy oxides with robust properties, metastable lattices, and precisely preserved multication compositions can be synthesized at relatively low temperatures.

3.3 Phase modulation and structural retention

Controlling the crystal structure of high-entropy oxides is of crucial significance for precisely regulating their electronic structure, oxygen vacancy chemical properties, and ionic transport behavior. The structural stability of these oxides under actual working conditions directly determines the long-term service performance of the materials. Due to the coexistence of multiple cations with different ionic radii and valence states in the same lattice, the competition among perovskite, spinel, perovskite-type, and fluorite-type crystal structures is particularly prominent. Therefore, single-phase high-entropy oxide products often find it difficult to stably exist. Configuration entropy, tolerance factors, and charge balance can be used as

key descriptive parameters to predict which phase is more likely to be stable in the system and the proximity of this phase to the phase boundary.[58–60] A deeper understanding of these laws drives the phase regulation strategies of high-entropy oxides from the traditional empirical trial-and-error mode to a more scientific and predictive design.

A typical example is the self-lattice framework strategy, in which the coordination preferences of cations are used to pre-design the target structure, while the Ga assistor can effectively reduce the phase's formation energy (Fig. 2f). By combining appropriate cation groups with the Ga assistor, ultra-thin high-entropy oxide nanosheets with phases such as rock salt, spinel, perovskite and fluorite phases have been obtained. This not only enables the controllable synthesis of the target phases but also effectively inhibits the formation of impurity phases.[61] The sol–gel method also provides an effective way for precise control of phases in the same composition system (Fig. 2g).[62] In the high-entropy LaB_5O_3 perovskite system, by increasing the complexity of the B-site cation composition, the system can be induced to transform from the tetragonal crystal system to the cubic crystal system, and this crystal transformation process is accompanied by an increase in the lattice distortion degree, an increase in oxygen vacancy concentration, and a synergistic optimization of nitrate reduction and sulfide oxidation performance.

Regulation strategies based on kinetic energy and strain offer diverse approaches for manipulating the phase and enhancing structural stability in HEOs. The flame spray pyrolysis technique enables the fabrication of single-phase high-entropy spinel nanoparticles within a millisecond time scale, where rapid quenching captures distorted spinel lattices with uniform cation distribution, an effect that is difficult to achieve *via* conventional slow solid-state sintering.[63,64]

Overall, these strategies show that configurational entropy, lattice distortion, kinetics and strain can be combined to select desired phases and keep them structurally robust under electrochemical and thermal stresses.

3.4 High-throughput and scalable manufacturing

As research on high-entropy oxides deepens, it has become clear that composition screening in these systems is highly complex. A typical multi-cation design space can contain hundreds or thousands of distinct compositions. The region that can be probed by conventional experiments represents only a very small portion of this space. When each composition also requires optimization of the synthesis conditions and microstructure, traditional one-by-one synthesis becomes prohibitively inefficient. Therefore, in recent years, to establish reliable links between the composition, structure, and performance, the focus of recent work has shifted from single-experiment and point-by-point optimization to a closed-loop mode that integrates parallel synthesis, rapid characterization, and data feedback. Within this framework, high-throughput strategies have emerged as key enablers. They allow systematic exploration of large composition libraries, generation of performance maps, and iterative refinement of promising candidates. At the same time, many of these methods are beginning to address the demand for scalable production.[65–67]

Rapid Joule heating synthesis represents a crucial step toward large-scale fabrication of HEOs. By directly applying an electric current to nickel foils coated with a precursor layer, high-entropy rock-salt, spinel, and perovskite oxides can crystallize within tens of seconds rather than hours, while retaining a single-phase structure and a high specific surface area.[68] The extremely steep thermal gradients and rapid cooling facilitate the inhibition of phase separation and enable the incorporation of elements that are difficult to stabilize under conventional calcination conditions, thereby expanding the accessible compositional space. Further studies on Joule-heated nanomaterials have demonstrated that this method can produce defect-rich, nanocrystalline high-entropy systems and related multimetallic nanoparticles with tunable grain sizes, highlighting the potential of integrating HEO synthesis with continuous production architectures.[69,70]

For thin-film architectures and device-oriented HEOs, combinatorial sputtering provides a prototypical high-throughput manufacturing strategy. A notable example is the fabrication of a Ba(Ti, Zr, Ta, Hf, Mo)O_3 high-entropy film library on Si using multi-cathode sputtering and a physical mask, which yields one hundred distinct metal–oxide-semiconductor capacitors on a single wafer.[71] Beyond single libraries, high-throughput sputtering and related combinatorial approaches are being generalized into modular discovery and scale-up pipelines. Perovskite La(XYZ)O_3 thin-film libraries prepared by combinatorial sputter deposition provide dense maps of phase fields and property landscapes, illustrating how multi-dimensional composition spaces can be navigated efficiently before committing to bulk synthesis.[72]

Researching new materials is often a complex process. High-throughput calculations can provide more accurate results. However, as material structures become more diverse and complex, relying solely on DFT-based high-throughput systems faces many challenges. This greatly limits the exploration of HER electrocatalysts.[73] Machine learning is an important modern technology. When combined with high-throughput calculations, it can build prediction models that are more efficient and accurate than DFT calculations.[74] This helps to quickly screen catalysts and discover new descriptors. In recent years, machine learning has become widely used as an efficient tool in computational materials science, with reports of its success in many fields.[75,76]

In summary, the high-throughput, scalable HEO manufacturing technology is evolving from the proof-of-concept stage to a multifunctional toolkit that integrates rapid synthesis, library-scale screening, and precise amplification for energy and electronic applications.

4. Advanced characterization and data-driven approaches for HEOs

HEOs have emerged as a unique class of materials with significant potential for a variety of applications, including energy

storage, catalysis, and electronics.[77] High-entropy oxides exhibit compositional complexity and intricate atomic configurations that render conventional *ex situ* characterization insufficient to resolve the atomistic origins of functional behavior. Realistic working environments impose dynamic changes in local coordination, oxidation state, defect population and surface adsorbates.[42] The complex and disordered structures of HEOs present challenges for traditional characterization techniques, requiring the development of advanced methods to probe their behavior and properties. This section discusses the roles of advanced techniques such as *in situ* infrared spectroscopy, *in situ* infrared imaging, theoretical calculations, and artificial intelligence (AI) in enhancing our understanding of HEOs. These techniques provide valuable insights into the structural, electronic, and catalytic properties of HEOs, thereby guiding the design of more efficient materials for practical applications.[78–80]

4.1 *In situ* vibrational spectroscopy

In situ vibrational spectroscopy provides direct access to surface intermediates, adsorbate configurations, and lattice dynamics of HEO catalysts under realistic operating conditions. Diffuse reflectance infrared Fourier transform spectroscopy (DRIFTS) and transmission infrared spectroscopy have been applied to HEOs. These spectra often exhibit broadened and asymmetric bands. Such features arise from the distribution of local cation environments and bond strengths, and these traits are intrinsic to multi-principal-element oxides. Time-resolved IR spectra under reactive flows make it possible to correlate spectral changes with catalytic performance in real time. Studies on nanofiber HEO catalysts under methane dry reforming conditions have shown that carbonate, bicarbonate and formate species form and transform dynamically on the surface (Fig. 3a–d).[47] The persistence of reactive carbon–oxygen species and the absence of strongly bound, inactive carbon deposits indicate that configurational entropy facilitates carbon removal and mitigates coking. These observations support the view that entropy-stabilized local structures modulate dehydrogenation and oxidation steps during high-temperature catalysis.

In situ FTIR and Raman spectroscopy were used to probe hydrothermal stability in spinel-type high-entropy oxides.[81] Under humid reaction atmospheres, vibrational spectra indicate a significantly reduced accumulation of surface hydroxyl groups compared to those of conventional binary spinels. This suppression of hydroxyl poisoning correlates strongly with improved catalytic stability. When interpreted alongside thermodynamic and structural analysis results, these spectroscopic results revealed that multication disorder lowers water adsorption affinity and facilitates rapid removal of surface hydroxyls. This combination of vibrational evidence provides a mechanistic explanation for why HEO catalysts maintain activity under moisture-rich conditions where conventional oxides deteriorate (Fig. 3e and f).

In situ DRIFTS has also been used to clarify the photocatalytic CO_2 hydrogenation mechanisms on fluorite-type HEOs.[82] During light-driven reactions, DRIFTS spectra capture the formation of formate, carbonate and CO-associated intermediates (Fig. 3g–l). The evolution process of these substances with changes in temperature and time indicates that the high configurational entropy will increase the concentration and heterogeneity of oxygen vacancy sites. These vacancy-related environments modulate the CO_2 adsorption geometry and hydrogenation behavior, resulting in enhanced CO and methanol production. Through *operando* spectral monitoring, DRIFTS provides mechanistic evidence linking entropy-driven defect chemistry to improved CO_2 hydrogenation performance.

4.2 *Operando* X-ray characterization

Operando X-ray absorption spectroscopy (XAS) has been widely used to probe the redox evolutions of multication HEO electrodes. In layered and rock-salt anodes, XAS measurements track the dynamic interconversion between metal oxidation states during lithiation and delithiation (Fig. 4a–f). HEOs display broad, overlapping features in their X-ray absorption near-edge structures because different cations exhibit distinct redox behaviors at different potentials. These spectra demonstrate that the conversion reactions typical of HEO electrodes involve synchronized but non-uniform contributions from multiple cation species, resulting in complex redox cascades.[83]

Complementary *operando* XRD provides insight into structural transformations during electrochemical cycling. In spinel-type HEO electrodes, *operando* XRD studies have shown reversible lattice expansions, phase transitions and conversion-to-rock-salt transformations under repeated cycling (Fig. 4g–k).[84] These features help explain the high capacity and also the structural fragility of such compositions. The simultaneous presence of multiple metal species leads to multi-step changes in diffraction peak positions, reflecting lattice distortions driven by compositional fluctuations.

4.3 First-principles calculations and multiscale simulations

First-principles calculations are indispensable for disentangling how configurational disorder, lattice distortion, and defect chemistry combine to determine the electronic and ionic transport properties of HEOs. Density functional theory (DFT), often extended with Hubbard U corrections or hybrid functionals, has been employed to compute defect formation energies, migration barriers, and band structures in prototypical entropy-stabilized oxides.[85] A new study on $(Mg_{0.2}Ni_{0.2}Co_{0.2}Cu_{0.2}Zn_{0.2})O$ has shown that both cation and oxygen vacancies tend to be deep defects with high ionization energies, indicating that shallow carrier doping is difficult to achieve.[86] By sampling thousands of local cation configurations around each defect using special quasi-random structures and statistical DFT workflows, these works have demonstrated that vacancy formation energies can vary by more than 1 eV depending on the local environment. This wide distribution explains why experimentally measured defect concentrations and transport coefficients often deviate from simple models based on a single average defect energy.

After modeling the OER performances of different compositions of AuIrOsPdPtReRhRu using machine learning (ML) models, it was found that AuIrOsPdRu was the best catalyst.[87]

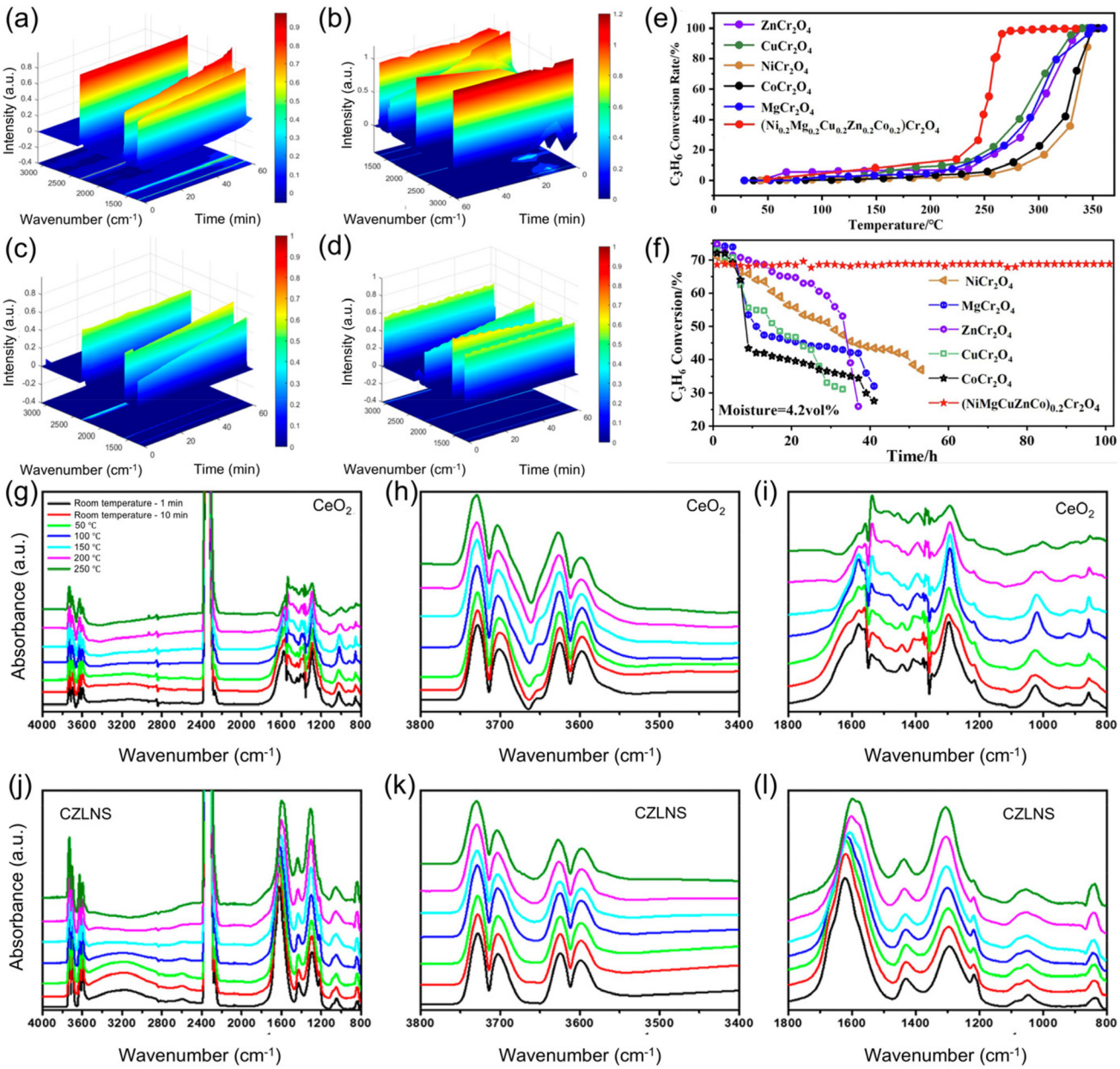

Fig. 3 *In situ* vibrational spectroscopy of HEO catalysts and their catalytic performance. (a–d) *In situ* DRIFTS spectra of CO_2 and CH_4 adsorption over high-entropy $(Ni_3MoCoZn)Al_{12}O_{24}$ nanofiber catalysts prepared by electrospinning (a and b) and their coprecipitated counterparts (c and d) during dry reforming of methane. Copyright 2024, American Chemical Society.[47] (e and f) C_3H_6 oxidation performance of spinel $(Ni_{0.2}Mg_{0.2}Cu_{0.2}Zn_{0.2}Co_{0.2})Cr_2O_4$ and single-component ACr_2O_4 (A = Zn, Cu, Ni, Co, Mg) catalysts, (20 000 mL h^{-1} g^{-1}; the feed gases contain 1vol% C_3H_6, 99 vol% air). (e) light-off curves under dry feed and (f) long-term stability tests in the presence of water vapor. Copyright 2024, Springer Nature.[81] (g–l) *In situ* DRIFTS spectra for photocatalytic CO_2 hydrogenation over ceria-based fluorite-type HEOs and CeO_2 at different temperatures and reaction times. Copyright 2024, American Chemical Society.[82]

Then, DFT was utilized to provide a complementary theoretical model with clear assumptions. DFT calculations indicated that most of the activity came from the Ru and Ir active sites, and the addition of Pd enhanced the performance of these sites. Overall, ML can help accelerate the discovery of catalysts, by combining ML models based on experimental data with DFT calculations models, providing important insights into the complex chemistry of OER catalysts.

From a catalytic perspective, DFT screening of adsorption energies and reaction barriers on model HEO surfaces provides mechanistic insight into synergistic effects. Such calculations often rely on reduced-complexity surface models where only a subset of cations is varied explicitly, but recent work is starting to integrate fully random cation distributions combined with configurational averaging to more faithfully represent HEO surfaces.[88]

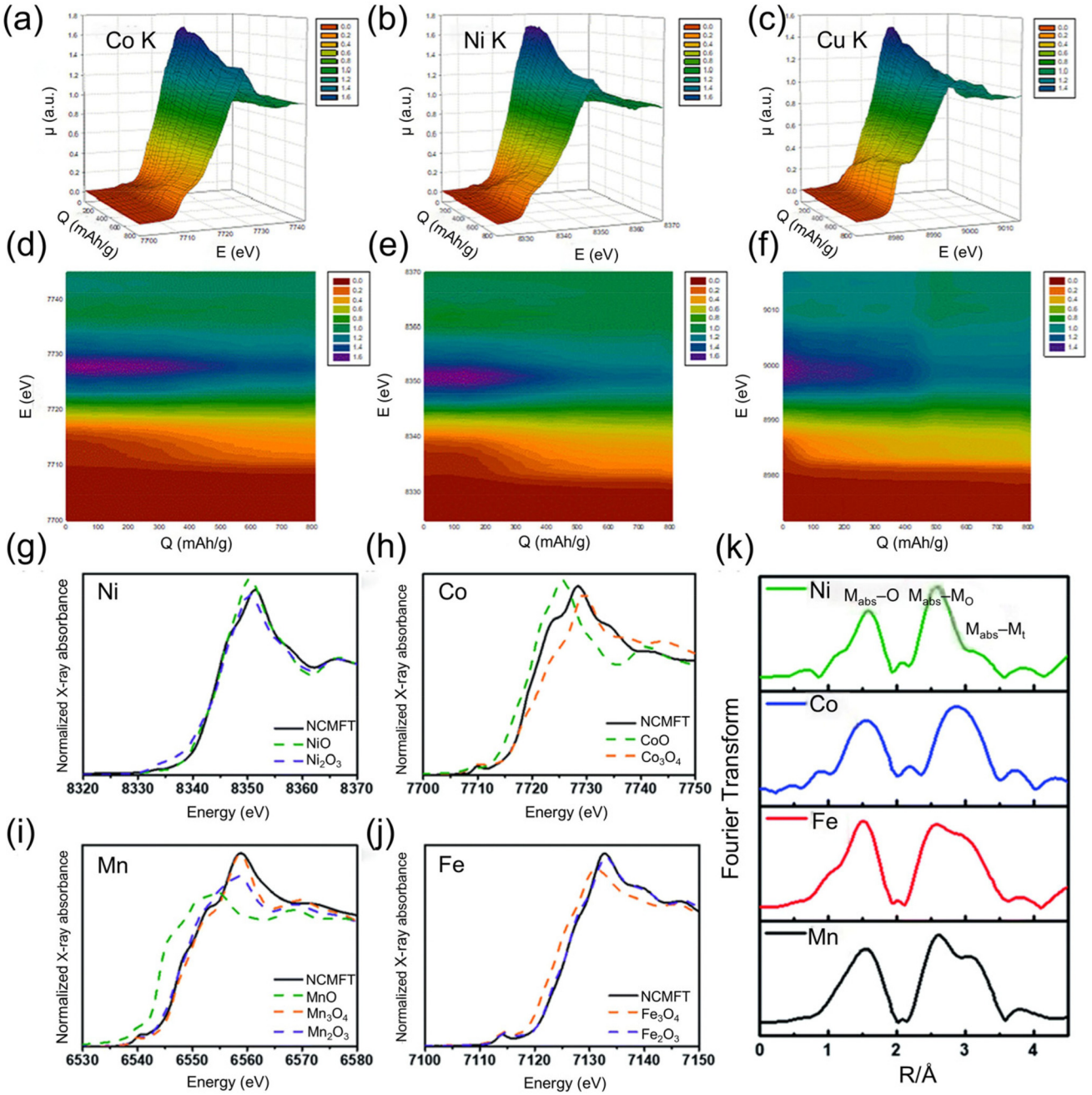

Fig. 4 *Operando* and *ex situ* X-ray absorption spectroscopy of high-entropy oxide anodes. (a–f) Co, Ni, and Cu K-edge XANES spectra in an operating HEO battery as a function of the delivered capacity in the lithiation process. Copyright 2020, American Chemical Society.[83] (g–j) Ni, Co, Mn, and Fe K-edge XANES spectra of spinel high-entropy oxide $(Ni_{0.2}Co_{0.2}Mn_{0.2}Fe_{0.2}Ti_{0.2})_3O_4$ (NCMFT). (k) Experimental Fourier transforms of the Ni, Co, Mn, and Fe K-edge EXAFS spectra of NCMFT. Copyright 2020, Royal Society of Chemistry.[84]

4.4 Artificial-intelligence accelerated approaches

AI has become essential in advancing HEO research. ML models can efficiently explore vast compositional spaces, allowing for the rapid identification of stable compositions and prediction of functional behaviors without the need for exhaustive experimental screening. By integrating AI with experimental data, researchers can predict material properties, optimize synthesis conditions, and refine catalytic mechanisms, thereby accelerating the development of HEOs for various applications. These AI-powered strategies not only shorten the discovery timeline but also help uncover previously inaccessible structure–property relationships, which are critical for the design of next-generation HEO materials.

ML is particularly well-suited to HEOs because of the vast size of the compositional design space. One recent study used

supervised learning models to accelerate the discovery of entropy-stabilized oxide catalysts for oxidation reactions.[89] The workflow combined a curated dataset of compositions, phase information and catalytic performance metrics with composition-derived descriptors such as cation electronegativity differences, ionic radius mismatch and valence electron configuration statistics. Models trained on this dataset were used to predict both phase stability and catalytic activity across large composition libraries. The ML-guided predictions identified composition regions with high probability of forming single-phase entropy-stabilized oxides that also exhibited superior oxidation activity. Targeted synthesis and testing confirmed many of these predictions, demonstrating a closed-loop cycle from data to model to experiment (Fig. 5a). This work provides a template for data-driven exploration of HEO catalysts that is significantly more efficient than manual trial-and-error.

ML has also been applied to multicomponent oxide electrocatalysts for the oxygen reduction reaction (ORR). Models trained on compositional and structural features have been used to predict ORR activity trends in multicomponent oxides and to identify compositional descriptors that correlate positively with the current density and onset potential (Fig. 5b).[90] These studies reinforce the notion that configurational entropy and cation diversity can be treated as quantitative design variables in catalyst optimization.

Moreover, ML methodologies have been extended to high-entropy cathodes for sodium-ion batteries and related energy-storage systems.[91] In these workflows (Fig. 5c), composition descriptors are combined with structural stability data and electrochemical performance metrics to train models that predict capacity retention, voltage profiles and structural robustness. The models highlight specific combinations of s-block and transition-metal cations that favor layered or polyanionic frameworks with good cycling stability.

ML interatomic potentials enable atomistic simulations of high-entropy oxides over supercell sizes and timescales that are prohibitive for conventional DFT. In one study, a machine-learning potential was constructed to reproduce energies and forces across a wide range of compositions and configurations for rock-salt HEOs.[92] The resulting model was then used to map mixing enthalpies, bond-length distributions and structural stability for thousands of candidate compositions. This approach identified known entropy-stabilized compositions and predicted additional stable or metastable candidates, illustrating the power of ML potentials for high-throughput

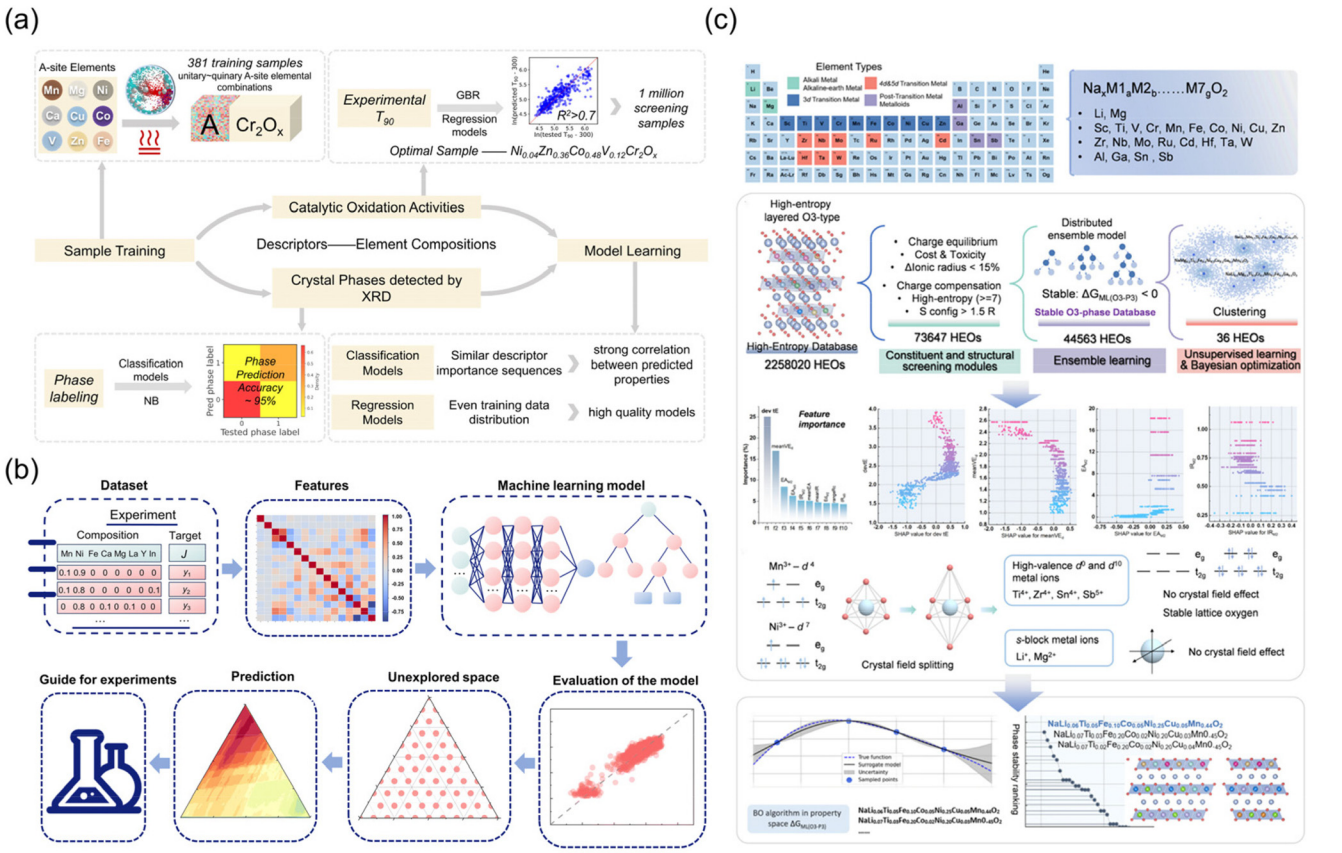

Fig. 5 Machine-learning strategies for the discovery and design of new HEO nanomaterials. (a) Schematic illustration of the ML approach employed to predict and acquire the structural and catalytic properties of the ACr_2O_x system. Copyright 2025, American Chemical Society.[89] (b) Operational workflow of the ML-driven analytical process utilized for investigating multicomponent ORR catalysts in alkaline environments. Copyright 2024, Royal Society of Chemistry.[90] (c) Hybrid-flow ML framework for designing high-entropy layered Na-ion cathodes. Copyright 2025, Wiley-VCH.[91]

computational screening. Combined with thermodynamic modelling and experimental validation, such tools can greatly expand the accessible HEO design space.

5. Catalytic applications of HEO nanomaterials

5.1 Thermal catalysis

High entropy oxides offer a dense population of cation configurations and defect motifs that can be exploited in thermally driven reactions such as CO_2 hydrogenation, CO oxidation, and tandem dehydrogenation–hydrogenation processes. The compositional complexity stabilizes redox active cations and oxygen vacancies at high temperature and at the same time provides multiple adsorption geometries for the reactants and intermediates. These traits are particularly valuable under harsh conditions where conventional single or binary oxides suffer from sintering, phase segregation, or poisoning.[93]

5.1.1 CO_2 hydrogenation. High entropy oxides are particularly attractive in CO_2 hydrogenation, where high temperatures and redox cycling often destroy conventional supported metals. The $Zr_{0.5}(NiFeCuMnCo)_{0.5}O_x$ nanomaterial has been used as a model system to investigate the dynamic behavior of supported nanoparticles during CO_2 hydrogenation.[94] Under hydrogen, Cu and other late transition metals exsolve from the high entropy matrix (Fig. 6a). When the gas phase switches back to oxidizing conditions, these particles dissolve into the oxide again. This reversible exsolution and dissolution process maintains a population of finely dispersed metal sites and slows down sintering that would normally deactivate the catalyst. The CO_2 conversion remains almost unchanged after many redox cycles because the active metals continuously regenerate from the entropy stabilized host (Fig. 6b).

The same design philosophy appears in other redox active HEOs. Spinel type $Co_3MnNiCuZnO_x$ nanoparticles can generate CuCoNi nanoalloys at the surface under reducing conditions and re-incorporate them when the gas feed becomes oxidizing. This dynamic exchange maintains a high density of metal–oxide interfaces and protects small particles from coalescence, which leads to sintering resistant performance in CO_2 conversion and related redox reactions.[95]

In parallel, fluorite structured high entropy oxides containing Zr, Y, and multiple transition metals have been used as hosts for isolated Pd species. In these materials, configurational entropy stabilizes atomically dispersed Pd–O complexes that hydrogenate CO_2 to formate through a non-classical pathway, achieving high turnover frequency and selectivity to formic acid under relatively mild conditions.[96]

A complementary strategy uses a family of high entropy oxides in which the relative amount of Fe is systematically varied. Non equimolar compositions based on Cr, Co, Mn, Ni, and Fe form highly crystalline oxides with controlled oxygen vacancy concentrations. These materials afford high methane yields and maintain their structures after long term CO_2 methanation, which is attributed to the balance between reducible Fe rich motifs and more stable cation environments.[97]

5.1.2 CO oxidation. Carbon monoxide oxidation is a classic probe reaction to test the oxygen activation ability and thermal robustness of oxide catalysts. Entropy-stabilized metal oxide solid solutions that combine Pt, Ni, Mg, Cu, Zn, and Co within a single rocksalt lattice reach complete CO conversion near room temperature and preserve activity after calcination at 900 °C. High configurational entropy maintains a uniform solid solution and prevents phase separation into less active

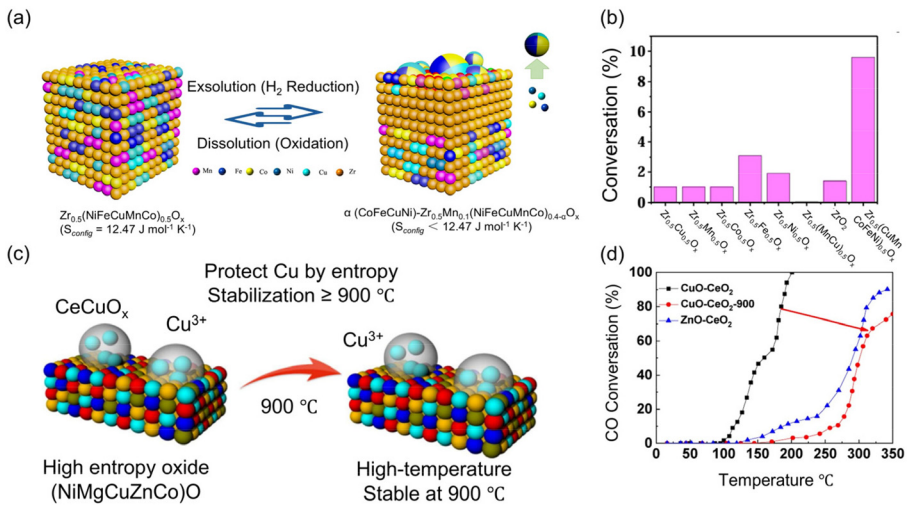

Fig. 6 High entropy oxide catalysts for thermally driven reactions. (a) Schematic illustration of *in situ* exsolution and dissolution of CoFeCuNi alloy nanoparticles from the high-entropy $Zr_{0.5}(NiFeCuMnCo)_{0.5}O_x$ host under H_2 reduction and oxidative treatment. (b) Catalytic performance of $Zr_{0.5}Cu_{0.5}O_x$, $Zr_{0.5}Mn_{0.5}O_x$, $Zr_{0.5}Co_{0.5}O_x$, $Zr_{0.5}Ni_{0.5}O_x$, $Zr_{0.5}Fe_{0.5}O_x$, $Zr_{0.5}(CuMn)_{0.5}O_x$, and $Zr_{0.5}(NiFeCuMnCo)_{0.5}O_x$ in CO_2 hydrogenation at 400 °C. Copyright 2021, Springer Nature.[94] (c) The effect of the $CuCeO_x$-HEO hetero-structure on the outstanding high-temperature stability during CO oxidation. (d) The temperature-dependent conversion of CO for CuO-CeO_2, ZnO-CeO_2 and Cu-ZnOx-CeO_2. Copyright 2020, Elsevier.[100]

binary oxides, while *in situ* microscopy reveals that noble metal and base metal cations remain highly dispersed even after harsh thermal cycling.[98] A high entropy oxide with the composition $(CeLaPrSmY)O_{2-y}$ shows high CO oxidation activity without precious metals. Different from traditional catalysts, HEOs can retain a single-phase structure even under high-temperature conditions, and their catalytic activity does not require the addition of costly platinum group metals.[99]

Heterostructured architectures that combine HEO domains with conventional oxides provide additional ways to regulate oxygen mobility. In the $CuO–CeO_2$ system, a high entropy (NiMgCuZnCo)O support can be interfaced with ceria to form a multiscale composite.[100] The entropy stabilized oxide anchors copper species and restrains their sintering, while the CeO_2 phase offers fast oxygen transport. After aging at 900 °C, the heterostructured catalyst retains high CO conversion and displays delayed deactivation compared with low entropy references. The high-entropy (NiMgCuZnCo)O layer encapsulates the $CeCuO_x$ aggregates and restricts their mobility during the high-temperature treatment process (Fig. 6c). The CO conversion rate curve indicates that the composite material based on HEO has superior stability compared to the traditional $CuO–CeO_2$ catalyst (Fig. 6d).

HEOs serve as thermally stable oxygen activation platforms, achieving low activation temperatures and sintering resistance through the configuration of entropy, high oxygen vacancies, and engineered HEO-oxide interfaces, thereby reducing reliance on precious metals.

5.1.3 Tandem dehydrogenation and hydrogen transfer reactions. Beyond simple oxidation and reduction reactions, high entropy oxides are emerging as platforms for tandem transformations that require multiple active functions. A representative case is the coupling of cyclohexanol dehydrogenation with acetone hydrogenation. In the system derived from $Cu_{0.75}Zn_{0.15}Mg_{7.1}Al_1Sc_1O_{11}$-HEO high entropy oxide, thermal reduction produces well dispersed Cu nanoparticles that remain strongly anchored to a multi-cation oxide matrix.[101] Cu sites promote O–H and C–H bond cleavage in cyclohexanol. Neighboring ZnO, MgO, Al_2O_3 and Sc_2O_3 like domains stabilize alkoxide intermediates and shuttle hydrogen through a spillover pathway that eventually drives acetone reduction. Under low weight hourly space velocity (WHSV), it is hypothesized that the active hydrogen species may be transformed into hydrogen gas and desorbed from the catalyst surface. At higher WHSV, acetone lacks sufficient time for complete reaction with the active hydrogen species, thus reducing the hydrogen transfer efficiency.

5.2 Electrocatalysis and rechargeable batteries

HEOs leverage their configurational entropy to not only stabilize multi-component single-phase structures but also enable extensive tunability of electronic structures and defect chemistry, establishing them as a versatile platform for electrochemical energy conversion and storage. Furthermore, HEOs exhibit exceptional structural stability under potential cycling, a broad design space for modulating adsorption energies, and decoupled activity-stability properties *via* the selective distribution of functional species across distinct cation sublattices. These attributes have prompted extensive and in-depth investigations into HEOs within the fields of electrocatalysis and energy materials.[88,102]

In electrocatalytic reactions, the multi-component cation sublattice allows synchronous optimization of metal–oxygen covalency, thereby tuning the distribution of key intermediates such as *OH, *O, and *OOH. Rock-salt, spinel, perovskite, and layered HEOs have demonstrated correlated behaviors in the OER, ORR, nitrate reduction reaction (NO_3^-RR), and battery electrode performance.[103] This design strategy is equally applicable to rechargeable battery systems, wherein lattice distortion, sluggish diffusion kinetics, and the "cocktail effect" markedly influence redox potentials, ion diffusion pathways, and mechanical stability during repeated intercalation processes. The following sections will focus on the mechanistic insights and performance of HEOs in oxygen electrocatalysis, nitrate reduction reactions, as well as lithium-, sodium-, and zinc-based battery systems.

5.2.1 Oxygen electrocatalysis. Spinel-type and perovskite-type HEOs have been extensively studied as OER catalysts.[104] A representative study on metal–organic framework (MOF)-derived HEOs demonstrated that converting polymetallic frameworks into nanoscale high-entropy oxides achieves a large surface area, high-density exposed active sites, and increased oxygen vacancies, collectively facilitating charge transfer and the exposure of coordination-unsaturated metal–oxygen sites. Compared to their low-entropy counterparts, these materials exhibit significantly reduced overpotentials and outstanding OER catalytic performance.[105]

High-entropy oxides with tailored oxygen vacancies have been synthesized through non-equilibrium thermal shock. The FeCoNiCrCuO HEO with an oxygen-vacancy-rich surface exhibited an overpotential of about 256 mV at 10 mA cm^{-2} in alkaline media (Fig. 7b) and a small Tafel slope (Fig. 7c). The four-electron transfer process of the OER was calculated using density functional theory to determine its free energy change (Fig. 7a). The results proved that the presence of oxygen deficiency is beneficial to the OER process.[106]

HEOs are frequently used as model systems to investigate the structure–activity relationships of the OER. Research on high-entropy OER catalysts based on oxide frameworks shared by multiple transition metals demonstrates that the coexistence of various cations can broaden the d-orbital range, reduce orbital degeneracy, and optimize the distribution characteristics of surface binding energy. This results in their significantly enhanced intrinsic activity and stability in overall water splitting compared to those of their single-metal or binary-metal-based counterparts.[107]

HEOs can also decouple oxygen redox reactions from structural degradation. A recent study on high-entropy-induced electric dipole transitions constructed bipolar dual-active sites in multi-component oxides (Fig. 7d), achieving reversible oxygen redox reactions (Fig. 7e) while mitigating the coupling effect between surface lattice oxygen oxidation and bulk structural

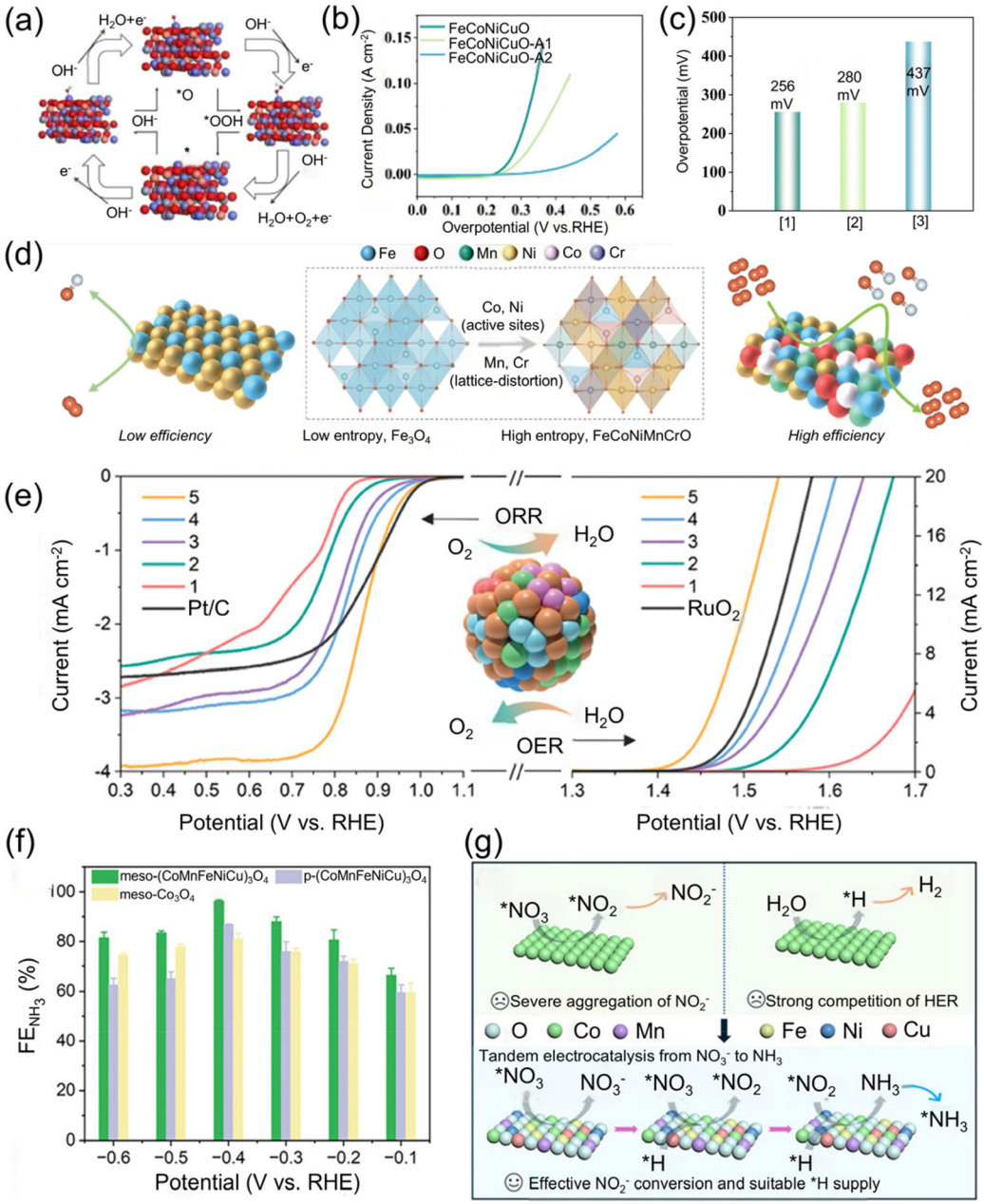

Fig. 7 HEOs for electrocatalysis. (a) OER mechanism on the oxygen-vacancy-rich FeCoNiCrCuO in alkaline medium (1 M KOH; Fe: purple spheres, Co: blue spheres, Ni: blue-gray spheres, Cr: gray spheres, Cu: orange spheres, and O: red spheres). (b) Linear sweep voltammetry scans for FeCoNiCrCuO, FeCoNiCrCuO-A1 and FeCoNiCrCuO-A2. (c) Comparison of overpotentials at 10 mA cm^{-2} for the three catalysts ([1] FeCoNiCrCuO, [2] FeCoNiCrCuO-A1, and [3] FeCoNiCrCuO-A2). Copyright 2025, Elsevier.[106] (d) Characteristics of low-entropy spinel oxide with integrated single octahedral sites and high-entropy spinel oxide with bipolar dual-active sites for the OER/ORR. (e) ORR/OER performances of spinel oxides and commercial catalysts (Pt/C and RuO_2) in 1 M KOH at a rotating speed of 1600 rpm. Copyright 2024, Wiley-VCH.[108] (f) $FENH_3$ values of p-$(CoMnFeNiCu)_3O_4$, meso-$(CoMnFeNiCu)_3O_4$ and meso-Co_3O_4. (g) Tandem electrocatalytic NO_3^--to-NH_3 mechanism of meso-$(CoMnFeNiCu)_3O_4$. Copyright 2025, Wiley-VCH.[110]

collapse.[108] The dual-active site design balances the redox processes of transition metal centers and oxygen centers. This mechanism is not only closely related to the OER but also applicable to the cathode operation of oxygen redox-active batteries. In catalysis, such bipolar sites can facilitate adsorption and desorption in oxygen electrocatalysis, providing a new approach to simultaneously enhance the OER and ORR on the same high-entropy oxide surface.

For the ORR, high-entropy spinel-type oxides have been reported as efficient cathode catalysts in metal–air configurations. In multicomponent spinels designed for the alkaline ORR, homogeneous distribution of several transition metals in

octahedral and tetrahedral sites improves the number and accessibility of redox-active centers, while the strong lattice distortion maintains structural integrity under large potential windows.[109] When integrated into zinc–air battery cathodes, such HEOs deliver high half-wave potentials ($E_{1/2}$) and superior cycling stability compared with conventional perovskites or noble-metal catalysts, demonstrating the promise of HEOs as bifunctional air electrodes coupling the ORR and OER.

In the field of oxygen electrocatalysis, the mapping of composition–activity relationships has progressively advanced through high-throughput experiments and computational simulations of the HEO space. A recent study systematically explored the composition-combination space of polycationic oxides, revealing intrinsic correlations among the local structure, electronic occupation states, and OER activity across numerous HEO systems.[87] Such data-driven research methodologies are well-suited to the inherently high-dimensional design space of HEOs, potentially accelerating the screening of optimal compositions for the ORR, OER, and related electrocatalytic processes.

5.2.2 Nitrate reduction to ammonia. The NO_3^-RR represents a key pathway for sustainable ammonia synthesis under mild conditions. The reaction typically involves complex tandem steps with relatively low selectivity. High-entropy mesoporous oxides provide an ideal platform for modulating adsorption energies along these pathways. $(CoMnFeNiCu)_3O_4$ significantly reduces the energy barrier for the hydrogenation–deoxygenation pathway in the NO_3^-RR, enabling highly selective ammonia synthesis in alkaline solutions.[110] The mesoporous HEO catalyst in this study exhibits a faradaic efficiency approaching 96% (Fig. 7f) and an ammonia yield exceeding 1.8 $mmol{\cdot}h^{-1}{\cdot}mg^{-1}$, outperforming single-metal oxides and low-entropy control samples. The high-entropy effect in this system finely tunes the local coordination environment, synergistically optimising nitrate adsorption, intermediate hydrogenation, and N–O bond cleavage. Such tandem schemes underscore the multifunctional potential of HEOs as both NO_3^-RR catalysts and anodic oxidation catalysts in paired electrosynthesis (Fig. 7g).

5.2.3 Lithium-ion batteries. In lithium-ion batteries (LIBs), HEOs primarily serve as conversion-type or insertion-type anodes, drawing significant attention because of their structural stability and strain-buffering capabilities.[111] A spinel-type HEO with the composition $(FeNiCrMnMgAl)_3O_4$ acts as a cyclically stable anode material in LIBs (Fig. 8a).[112] This polycationic spinel exhibits high cyclability (Fig. 8b) and reversible discharge performance (Fig. 8c), with activation processes, lattice distortion, and abundant oxygen vacancies facilitating charge-transport kinetics.

Moreover, HEO structures shorten lithium-ion diffusion pathways, expand the contact area between electrodes and electrolytes, and increase internal voids. Such voids effectively mitigate volume expansion during cycling. The high-entropy lattice constructs a spatial support network for lithium insertion/extraction processes, safeguarding structural integrity throughout material cycling and ultimately conferring exceptional cycling stability.[113,114]

Polyacrylonitrile (PAN) was employed as a binder to form a cyclised polyacrylonitrile (cPAN) outer layer on the NHEO surface (NHEO-cPAN) *via* an *in situ* thermochemical cyclisation reaction (Fig. 8d).[115] The *in situ*-formed cyclic polyacrylonitrile coating not only enhances electrical conductivity but also improves structural and interfacial stability. The resulting NHEO-cPAN electrode exhibits significantly enhanced rate performance and cycling stability (Fig. 8e). This study demonstrates that combining the high-entropy design of bulk materials with tailored surface layers represents an effective pathway for developing commercially viable HEO-based lithium-ion battery anodes.

5.2.4 Sodium-ion batteries. High-entropy layered oxides have emerged as promising sodium-ion battery (SIB) cathode materials, attracting intense interest. Sodium insertion hosts suffer from more severe phase transitions and air instability than their lithium counterparts; a high-entropy design alleviates detrimental phase transitions, enhances Na^+ diffusion kinetics, and sustains the layered framework stability during long-term cycling.[116] The high-entropy effect expands the configurational space for cation ordering. It flattens the potential landscape to facilitate Na^+ migration along two-dimensional diffusion pathways.

These concepts have been applied to practical cathode designs. A high-entropy O_3-$Na_{0.95}Li_{0.06}Ni_{0.25}Cu_{0.05}Fe_{0.15}Mn_{0.49}O_2$ cathode for solid-state SIBs (Fig. 8f) delivered high reversible capacity, exceptional rate capability and long-term cycling stability (Fig. 8g–i).[117] Incorporating multiple transition metals and Li^+ into the O_3 lattice alleviates lattice stress and boosts ionic conductivity. This enables rapid, reversible O_3–P_3 phase transition while inhibiting irreversible structural alterations. Structural characterization techniques such as high-resolution electron microscopy and *in situ* monitoring uncovered homogeneous element distribution and robust lattice evolution under high-rate cycling. These features represent the signature advantages of high-entropy design.

High-entropy layered oxide cathodes for SIBs have been shown to combine high Na content, favorable redox potentials and improved structural integrity, making them promising candidates for large-scale stationary applications where cost and resource abundance are crucial. Design guidelines emerging from these studies stress the importance of carefully selecting transition-metal combinations and dopants to balance charge compensation, oxygen redox participation and mechanical stability.[118]

5.2.5 Zinc-ion batteries. For aqueous zinc-ion batteries (ZIBs), cathode stability during Zn^{2+} intercalation/deintercalation is a major challenge, and high-entropy oxides offer a route to suppress structural collapse. A spinel-type high-entropy oxide cathode $(Co_{0.2}Cr_{0.2}Fe_{0.2}Mn_{0.2}Ni_{0.2})_3O_4$ (CCFMnO) was used as a cathode material for aqueous ZIBs. The high-entropy cathode exhibited an excellent specific capacity of 283 $mAh{\cdot}g^{-1}$ at low current density and maintained more than 66% of its capacity after 90 000 cycles at 2 $A{\cdot}g^{-1}$.[119]

The concept of high entropy has been further extended to the design principles of ZIB materials, encompassing both

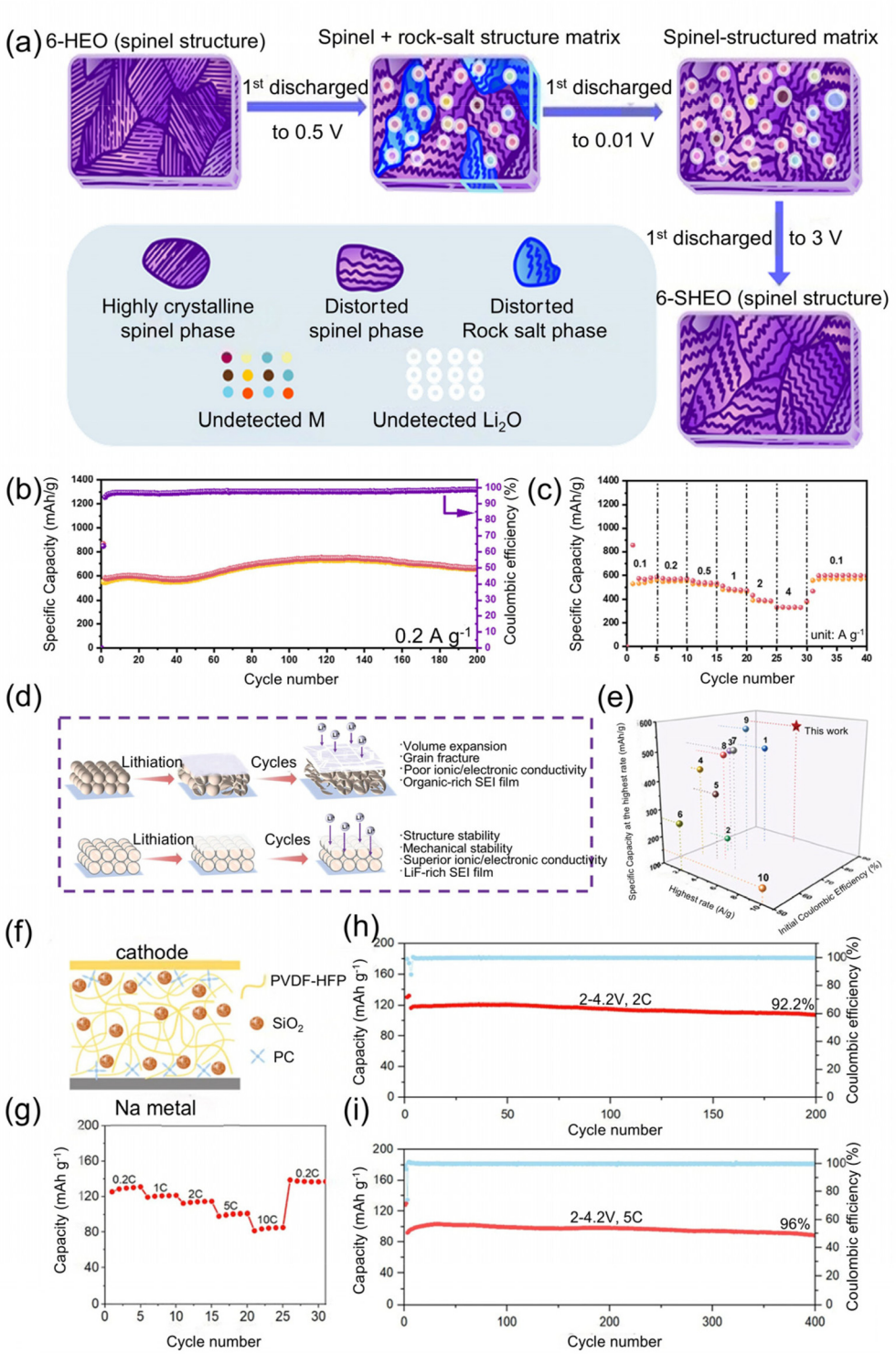

Fig. 8 High-entropy oxide electrodes for rechargeable batteries. (a) Schematic illustration of the lithium-storage mechanism of the spinel-type 6-SHEO anode, showing the reversible evolution among highly crystalline spinel, distorted spinel, and distorted rock-salt phases during the first discharge/charge process. (b) Long-term cycling performance and coulombic efficiency of the 6-SHEO anode at 0.2 $A \cdot g^{-1}$. (c) Rate capability of 6-SHEO at different current densities. Copyright 2022, MDPI.[112] (d) Schematic comparison of structural evolution and solid-electrolyte interphase formation for NHEO-PVDF and NHEO-PAN500 electrodes upon repeated lithiation. (e) Radar plot comparing capacity, rate performance, cycling stability and related metrics of NHEO-PAN500 with representative conversion-type anodes. Copyright 2024, Wiley-VCH.[115] (f) Schematic configuration of a solid-state sodium-ion battery employing an O_3-type $Na_{0.95}Li_{0.06}Ni_{0.25}Cu_{0.05}Fe_{0.15}Mn_{0.49}O_2$ high-entropy layered cathode and a PVDF-HFP/SiO_2/PC polymer solid electrolyte. (g) Rate performance of the $Na_{0.95}$LNCFM polymer solid-state battery at various C-rates. (h and i) Long-term cycling performance and coulombic efficiency of the $Na_{0.95}$LNCFM PSE battery at 2C and 5C. Copyright 2023, Springer.[117]

electrode and electrolyte components. The high-entropy material design philosophy for ZIBs indicates that high-entropy doping or multi-cationic frameworks can optimize diffusion pathways, regulate solvation structures, and alleviate local stresses.[120] When combined with *in situ* characterization, these designs reveal that distributing redox and structural roles among multiple cations reduces the likelihood of catastrophic phase transitions and allows more homogeneous Zn^{2+} insertion, which is essential for long-term durability in aqueous environments.

By merging high-entropy structural design with detailed mechanistic understanding from *operando* methods, HEO-based ZIB cathodes are moving toward practical performance targets for grid-scale storage.

5.3 Photocatalysis

HEOs are increasingly used as multifunctional photocatalysts, because the disordered cation lattice combines broad optical absorption with dense distributions of redox-active sites and abundant defects. Compared with conventional single-component oxides, the configurational entropy in these materials stabilizes complex compositions and allows band structures to be tuned through collective variations of several cations at once. Such band-gap engineering and defect control can be exploited across water splitting, carbon dioxide reduction, and pollutant removal, while maintaining structural robustness under continuous illumination and harsh solution conditions.[43,121,122]

5.3.1 Water splitting. Early studies on solar-driven hydrogen production have shown that compositionally complex, single-phase high-entropy oxides can operate as intrinsically active photocatalysts. The initial high-entropy photocatalyst was fabricated through mechanical alloying using the high-pressure torsion (HPT) method, followed by high-temperature oxidation. The biphasic oxide with an overall composition of $TiHfZrNbTaO_{11}$ has successfully achieved hydrogen generation *via* photocatalytic water splitting, indicating that HEOs hold promise as novel low-bandgap photocatalysts.[123] More recent studies on $TiZrNbHfTaO_x$ have extended this strategy to near-neutral aqueous media and visible irradiation, where mechano-thermal synthesis produced nanocrystalline high-entropy oxides that deliver competitive hydrogen evolution rates without noble metals. Such results not only present a novel approach for fabricating high-entropy photocatalysts but also verify the great promise of such materials in hydrogen production without relying on precious metal co-catalysts.[124]

5.3.2 Hydrogen peroxide production. There is an octonary rutile-type high-entropy oxide containing Ti, V, Cr, Nb, Mo, W, Cu, and Al for direct photocatalytic hydrogen peroxide production from water and atmospheric O_2.[125] The material integrates light harvesting and catalytic functions in a single rutile phase. Oxygen vacancies generate intermediate band states within the wide band gap, thus extending the absorption range from the ultraviolet to the near-infrared region and enabling full-spectrum solar energy utilization of TVCNWCA-HEO. Density-functional calculations reveal that water adsorption on Mo and W sites near oxygen vacancies induces strong charge redistribution and spontaneous formation of surface hydroxyl species, which lowers the barrier for the two-electron water oxidation pathway that yields hydrogen peroxide rather than oxygen (Fig. 9a). Oxygen molecules adsorb at V and Cu sites through both Griffiths-type and Pauling-type configurations, and the weakened O–O bond at these sites facilitates the formation of *OOH intermediates along the two-electron oxygen reduction route (Fig. 9b). Kinetic analysis under visible light shows that the octonary high-entropy oxide generates about 21 millimolar hydrogen peroxide within one hour without sacrificial reagents (Fig. 9c). These trends confirm that both the high configurational entropy and the specific combination of cations are necessary to balance water oxidation and oxygen reduction steps and to stabilize oxygen-vacancy-rich surfaces.

5.3.3 Degradation of organic pollutants and antibiotics. High-entropy oxides have also been applied as photocatalysts for environmental remediation, where the combination of multielement active sites and robust defect structures benefits the degradation of recalcitrant contaminants. Single-phase $Gd_{0.2}La_{0.2}Ce_{0.2}Hf_{0.2}Zr_{0.2}O_2$ and $Gd_{0.2}La_{0.2}Y_{0.2}Hf_{0.2}Zr_{0.2}O_2$ multi-component oxide nanoparticles exhibit efficient visible-light-driven reduction of hexavalent chromium and decomposition of methylene blue (MB) dye. Their activity has been attributed to a synergy between lattice distortion, mixed valence states, and defect-mediated charge separation.[126] Follow-up work on the single-phase cubic fluorite $(CeGdHfPrZr)O_2$ nanoparticles proved that they serve as reusable photocatalysts in MB dye degradation. They retain degradation performance after multiple cycles, because the entropy-stabilized lattice prevents dissolution and phase segregation.[127]

$(La_{0.2}Ce_{0.2}Gd_{0.2}Zr_{0.2}Fe_{0.05})O_2$ nanoparticles confirmed that the material exhibits photocatalytic degradation of tetracycline hydrochloride. Its superior performance provides another route to improve photocatalytic degradation, as controlled introduction of Fe cations and associated oxygen vacancies produces higher carrier densities and more adsorption sites for pollutants.[128] Layered bismuth-based high-entropy oxides extend this concept to two-dimensional architectures. These materials offer internal electric fields and exposed bismuth-oxygen motifs that cooperate to accelerate photogenerated carrier separation, leading to efficient degradation of methyl orange.[129] Across these investigations, the multicomponent oxide matrix expands the absorption range. It provides diverse adsorption configurations for pollutants and reactive oxygen intermediates, enabling multiple oxidative pathways to proceed simultaneously.

Magnetic high-entropy spinel oxides offer promising potential for practical water treatment. Spinel $(FeCoNiCuZn)_aO_b$ nanoparticles, synthesized *via* thermal decomposition, exhibit strong visible-light absorption, abundant surface oxygen defects, and enhanced charge separation and transfer.[130] Under visible light, these nanoparticles effectively degrade sulfamethoxazole and ofloxacin within ninety minutes. Band

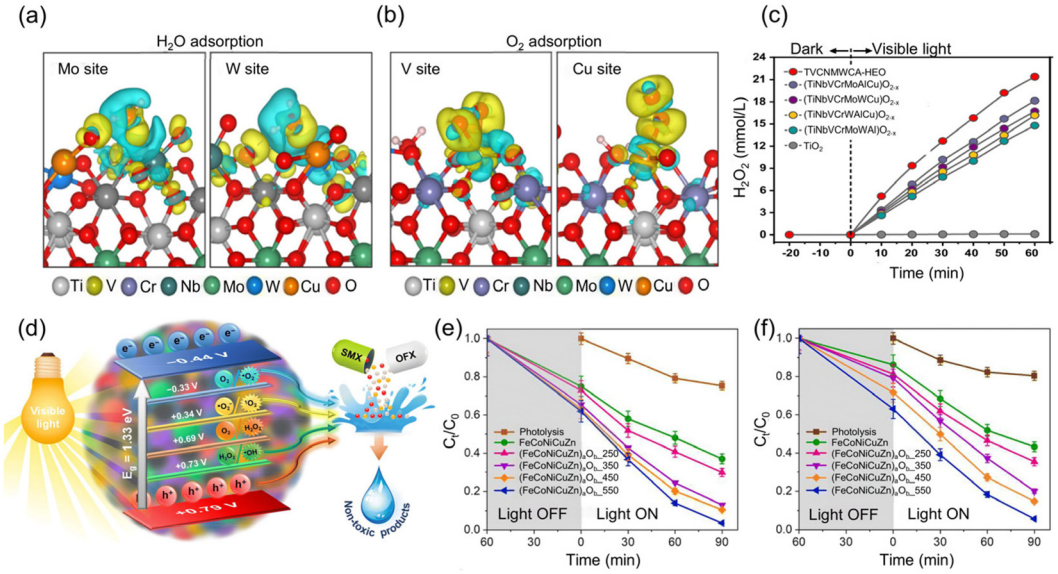

Fig. 9 High-entropy oxide photocatalysts for visible-light H_2O_2 production and antibiotic degradation. (a and b) Charge density difference plots for water and oxygen adsorption on representative cation sites of an octonary rutile-type TiVCrNbMoWCuAl high-entropy oxide. The visualized electron accumulation and depletion regions highlight how Mo and W sites favor water activation while V and Cu sites facilitate oxygen activation through distinct adsorption configurations. (c) Photocatalytic H_2O_2 production with TVCNMWCA-HEO, other septenary high-entropy oxides, and TiO_2 in pure water under visible light irradiation ($\lambda \geq 420$ nm, 300 mW cm^{-2}). Copyright 2024, Springer Nature.[125] (d) Schematic band structure and reaction pathway for visible-light-driven degradation of antibiotic pollutants over spinel $(FeCoNiCuZn)_aO_b$_550 NPs. Visible light-induced photocatalytic degradation of (e) sulfamethoxazole (SMX) and (f) ofloxacin (OFX) by FeCoNiCuZn and $(FeCoNiCuZn)_aO_b$ NPs. Copyright 2024, Royal Society of Chemistry.[130]

structure analysis shows that the conduction and valence bands align with the redox potentials necessary for $^{\bullet}O_2^-$ and $^{\bullet}OH$. As reactions take place on the surface, $^{\bullet}O_2^-$ and $^{\bullet}OH$ along with holes act on the antibiotic molecules adsorbed on the HEO NPs, finally breaking them down into simpler compounds (Fig. 9d). Photodegradation tests indicate that the high-entropy spinel outperforms both the parent multimetal alloy and simple oxide references. Concentration–time profiles demonstrate negligible pollutant loss in the dark, followed by rapid degradation under light, confirming a photocatalytic reaction rather than adsorptive processes (Fig. 9e and f).

These examples illustrate how compositional complexity, defect engineering, and magnetic functionality can be integrated within HEOs to deliver photocatalysts that couple strong and tunable light absorption with robust redox activity and convenient separation. Insights from water splitting, hydrogen peroxide generation, and pollutant degradation point to common design principles. These include constructing high-entropy lattices that stabilize dense oxygen vacancies, distributing multiple cation species to create a spectrum of adsorption sites for reactants and intermediates, and using band-gap engineering to align semiconductor levels with targeted redox couples.

6. Challenges and perspectives

HEOs have emerged as a novel class of materials with exceptional potential for a variety of catalytic and energy applications. They offer several advantages, including enhanced catalytic activity due to the presence of oxygen vacancies, multi-active components, and high thermal stability. These properties enable HEOs to outperform traditional materials in various catalytic reactions. Moreover, their versatility in energy storage and conversion further enhances their application potential.

However, despite these advantages, several challenges still need to be addressed to realize the potential of HEOs.

(1) Phase stability under operating conditions is still a key risk. Because the chemical potential of oxygen and surface adsorbates changes, the entropy-stabilized phases at synthesis temperature may transform during catalysis. Surface reconstruction, cation leaching, and redox-driven segregation can occur even when the bulk remains a single phase. Future work needs stability criteria that match operating, not only synthesis phase purity.

(2) Machine learning is becoming essential, but model transferability is a major challenge for HEOs. It can accelerate the exploration of HEO configuration space by learning structure–property relationships and by guiding where to sample next. Recent work also shows the potential of machine-learning interatomic potentials to study disorder and stability beyond conventional DFT limits. Still, robust performance requires curated datasets, physically meaningful descriptors, and validation across synthesis routes and measurement platforms.

(3) HEOs often require tight control over composition uniformity, oxidation states, and defect populations. These targets

become harder to maintain when synthesis is scaled up from milligram powders to gram-scale batches, or when materials are transferred from thin-film libraries to bulk catalysts. Small changes in precursor chemistry, heating profiles, and mass transport can cause composition drift, local segregation, or morphology collapse. These variations reduce reproducibility across laboratories and limit practical translation. Future work should focus on process–structure mapping and on reporting synthesis windows with clear tolerances. It is also important to validate that the composition, phase, and defect descriptors remain consistent after scale-up and after shaping into electrodes or devices. This scale-up validation is increasingly viewed as a key step for moving HEOs from discovery to application.

The future of HEOs holds great promise, particularly as advancements in synthesis techniques and mechanistic understanding continue. Looking forward, further investigation into the atomic-level structure and active sites by integrating advanced characterization techniques with computational tools such as DFT and ML will provide new insights into understanding their outstanding catalytic performance. Understanding these mechanisms will enable the rational design of HEOs tailored to specific applications, from catalysis to energy storage. At the same time, developing low-temperature and high-throughput synthesis methods will be essential for scaling up the production of HEOs, making them more cost-effective and widely accessible. HEOs also present an exciting opportunity for sustainable technologies, where they could replace expensive noble metals. As the stability and scalability of HEOs improve, their integration into industrial applications will become more feasible, helping to address both environmental and energy challenges.

Conflicts of interest

There are no conflicts to declare.

Data availability

No primary research results, software or code have been included and no new data were generated or analysed as part of this review.

Acknowledgements

This work was financially supported by the National Key Research and Development Program of China (2022YFA1505700), the National Natural Science Foundation of China (22475044), the Project of Qinglan Talent of Jiangsu and Pre-Research Fund of Ministry of Education of China (No. 8091B022212).

References

1 Y. Wang, M. Tang, Z. Lyu, W. Fu, H. Yan, S. Zhou, Y. Sun and Y. Dai, *Adv. Sci.*, 2025, **12**, 2501334.
2 J. W. Yeh, S. K. Chen, S. J. Lin, J. Y. Gan, T. S. Chin, T. T. Shun, C. H. Tsau and S. Y. Chang, *Adv. Eng. Mater.*, 2004, **6**, 299–303.
3 C. M. Rost, E. Sachet, T. Borman, A. Moballegh, E. C. Dickey, D. Hou, J. L. Jones, S. Curtarolo and J.-P. Maria, *Nat. Commun.*, 2015, **6**, 8485.
4 Y. Jiao, J. Dai, Z. Fan, J. Cheng, G. Zheng, L. Grema, J. Zhong, H.-F. Li and D. Wang, *Mater. Today*, 2024, **77**, 92–117.
5 S. Das, S. Chowdhury and C. S. Tiwary, *Nanoscale*, 2024, **16**, 8256–8272.
6 M. Moździerz, K. Świerczek, J. Dąbrowa, M. Gajewska, A. Hanc, Z. Feng, J. Cieślak, M. Kądziołka-Gaweł, J. Płotek, M. Marzec and A. Kulka, *ACS Appl. Mater. Interfaces*, 2022, **14**, 42057–42070.
7 Z.-Y. Liu, Y. Liu, Y. Xu, H. Zhang, Z. Shao, Z. Wang and H. Chen, *Green Energy Environ.*, 2023, **8**, 1341–1357.
8 M. Fu, X. Ma, K. Zhao, X. Li and D. Su, *iScience*, 2021, **24**, 102177.
9 Z. Hong, Z. C. Jian, Y. F. Zhu, Y. J. Li, Q. C. Ling, H. Xin, D. Wang, C. Wu and Y. Xiao, *Chem. Sci.*, 2025, **16**, 17058–17085.
10 Y. Shi, H. Zhang, G. Ren, W. Xiao, L. Li, Y. Hu, K. M. Reddy, X. Zhao, L. Zhu and N. Ni, *Acta Mater.*, 2024, **271**, 119906.
11 H. Xie, Z. Yang, J. Liu, W. Wu, T. Huang and H. Liu, *Chem. Commun.*, 2025, **61**, 10449–10469.
12 P. Cui, K. Peng, F. Miao and T. Gu, *Renewable Sustainable Energy Rev.*, 2026, **226**, 116301.
13 R. Hou, Y. Wei, J. Zhang, J. Chen, S. Chen, S. Sun, G. Shao and P. Zhang, *Adv. Sci.*, 2025, **12**, e11072.
14 L. He, H. Kang, G. Hou, X. Qiao, X. Jia, W. Qin and X. Wu, *Chem. Eng. J.*, 2023, **460**, 141675.
15 A. Güngör, E. Saritas, D. Toloman, A. Popa, A. M. Rostas and E. Erdem, *Nanoscale*, 2025, **17**, 26532–26557.
16 C. Oses, C. Toher and S. Curtarolo, *Nat. Rev. Mater.*, 2020, **5**, 295–309.
17 H. Leng, P. Zhang, J. Wu, T. Xu, H. Deng, P. Yang, S. Wang, J. Qiu, Z. Wu and S. Li, *Nanoscale*, 2023, **15**, 19139–19147.
18 M. Brahlek, M. Gazda, V. Keppens, A. R. Mazza, S. J. McCormack, A. Mielewczyk-Gryń, B. Musico, K. Page, C. M. Rost, S. B. Sinnott, C. Toher, T. Z. Ward and A. Yamamoto, *APL Mater.*, 2022, **10**, 110902.
19 S. J. McCormack and A. Navrotsky, *Acta Mater.*, 2021, **202**, 1–21.
20 H. Li, Y. Zhou, Z. Liang, H. Ning, X. Fu, Z. Xu, T. Qiu, W. Xu, R. Yao and J. Peng, *Coatings*, 2021, **11**, 628.
21 A. Sarkar, R. Djenadic, N. J. Usharani, K. P. Sanghvi, V. S. K. Chakravadhanula, A. S. Gandhi, H. Hahn and S. S. Bhattacharya, *J. Eur. Ceram. Soc.*, 2017, **37**, 747–754.
22 A. Kumar, D. Bérardan, F. Brisset, D. Dragoe and N. Dragoe, *J. Mater. Chem. A*, 2023, **11**, 14320–14332.
23 L. Xu, H. Wang, L. Su, D. Lu, K. Peng and H. Gao, *J. Eur. Ceram. Soc.*, 2021, **41**, 6670–6676.

24 X. Qi, Y. Gu, J. Yan, X. Liu and X. Zhang, *J. Inorg. Mater.*, 2021, **36**, 379–385.
25 Q. Yang, G. Wang, H. Wu, B. A. Beshiwork, D. Tian, S. Zhu, Y. Yang, X. Lu, Y. Ding, Y. Ling, Y. Chen and B. Lin, *J. Alloys Compd.*, 2021, **872**, 159633.
26 D. Stenzel, B. Zhou, C. Okafor, M. V. Kante, L. Lin, G. Melinte, T. Bergfeldt, M. Botros, H. Hahn, B. Breitung and S. Schweidler, *Front. Energy Res.*, 2022, **10**, 942314.
27 H. Chen, N. Qiu, B. Wu, Z. Yang, S. Sun and Y. Wang, *RSC Adv.*, 2020, **10**, 9736–9744.
28 L. Spiridigliozzi, C. Ferone, R. Cioffi and G. Dell'Agli, *Acta Mater.*, 2021, **202**, 181–189.
29 D. Berardan, A. K. Meena, S. Franger, C. Herrero and N. Dragoe, *J. Alloys Compd.*, 2017, **704**, 693–700.
30 J. Zou, L. Tang, W. He and X. Zhang, *ACS Nano*, 2024, **18**, 34492–34530.
31 S. S. I. Almishal, M. Furst, Y. Tan, J. T. Sivak, G. Bejger, J. Petruska, S. V. G. Ayyagari, D. Srikanth, N. Alem, C. M. Rost, S. B. Sinnott, L. Q. Chen and J. P. Maria, *Nat. Commun.*, 2025, **16**, 8211.
32 C. M. Rost, Z. Rak, D. W. Brenner and J. P. Maria, *J. Am. Ceram. Soc.*, 2017, **100**, 2732–2738.
33 Y. Guan, G. Zhou, Y. Jiang, J. Dong, L. Li, J. Yin, S. Huang, L. Zhang and E. H. Ang, *Sep. Purif. Technol.*, 2025, **358**, 130267.
34 X. Liu, P. Zhang, M. Huang, Y. Han, N. Xu, Y. Li, Z. Zhang, W. Pan and C. Wan, *J. Eur. Ceram. Soc.*, 2023, **43**, 6407–6415.
35 H. Wang, S. Ma, W. Zhao, Q. He, Y. Liu, S. Zhao and Y. Yang, *Mater. Res. Lett.*, 2024, **13**, 24–34.
36 J. Wang, S. Liu, M. Tang, W. Fu, Y. Wang, K. Yin and Y. Dai, *Small*, 2023, **19**, e2300547.
37 H. Nan, S. Lv, Z. Xu, Y. Feng, Y. Zhou, M. Liu, T. Wang, X. Liu, X. Hu and H. Tian, *Chem. Eng. J.*, 2023, **452**, 139501.
38 J. Hao, F. Ma, Y. Chen, S. Lu, F. Duan, M. Du, C. Wang, W. Zhang and H. Zhu, *New J. Chem.*, 2024, **48**, 511–514.
39 Y. Ma, Y. Ma, Q. Wang, S. Schweidler, M. Botros, T. Fu, H. Hahn, T. Brezesinski and B. Breitung, *Energy Environ. Sci.*, 2021, **14**, 2883–2905.
40 K. Y. Tsai, M. H. Tsai and J. W. Yeh, *Acta Mater.*, 2013, **61**, 4887–4897.
41 J. Dąbrowa, M. Zajusz, W. Kucza, G. Cieślak, K. Berent, T. Czeppe, T. Kulik and M. Danielewski, *J. Alloys Compd.*, 2019, **783**, 193–207.
42 S. Sen, M. Palabathuni, K. M. Ryan and S. Singh, *ACS Energy Lett.*, 2024, **9**, 3694–3718.
43 H. Tsubota, A. Jitianu and G. Kawamura, *ACS Mater. Lett.*, 2025, **7**, 1042–1056.
44 J. Yang, S. Gong, S. Liu, X. Wu, Z. Guo, Y. Zhao and C. Chen, *Nano Res.*, 2025, **18**, 94907774.
45 M. Rafique, T. Yao, S. Ma, Y. Xu, L. Li, J. Han, Q. Fu, W. Li, Z. Yuan, K. Wang and B. Song, *Adv. Funct. Mater.*, 2025, **36**, e12495.
46 Y. Gao, Y. Liu, H. Yu and D. Zou, *Appl. Catal., A*, 2022, **631**, 118478.
47 M. Zhang, J. Ye, Y. Gao, X. Duan, J. Zhao, S. Zhang, X. Lu, K. Luo, Q. Wang, Q. Niu, P. Zhang and S. Dai, *ACS Nano*, 2024, **18**, 1449–1463.
48 Y. Wang, Z. Lyu, Y. Xiao, L. Han, Y. Sun and Y. Dai, *Adv. Funct. Mater.*, 2025, e12568.
49 S. Nie, L. Wu, L. Zhao, X. Zheng, S. Yang and P. Zhang, *Chem. Catal.*, 2021, **1**, 648–662.
50 G. Wang, J. Qin, Y. Feng, B. Feng, S. Yang, Z. Wang, Y. Zhao and J. Wei, *ACS Appl. Mater. Interfaces*, 2020, **12**, 45155–45164.
51 G.-J. Lee, E.-K. Park, S.-A. Yang, J.-J. Park, S.-D. Bu and M.-K. Lee, *Sci. Rep.*, 2017, **7**, 46241.
52 A. Varma, A. S. Mukasyan, A. S. Rogachev and K. V. Manukyan, *Chem. Rev.*, 2016, **116**, 14493–14586.
53 Z. Luo and X. Zhou, *Sci. Adv.*, 2025, **11**, eadw1461.
54 Y. Chen, C. Guo, Y. Wang, K. Wang and S. Song, *Chin. J. Catal.*, 2025, **77**, 210–219.
55 D. Wang, Z. Liu, S. Du, Y. Zhang, H. Li, Z. Xiao, W. Chen, R. Chen, Y. Wang, Y. Zou and S. Wang, *J. Mater. Chem. A*, 2019, **7**, 24211–24216.
56 K. Iwase and I. Honma, *ACS Appl. Energy Mater.*, 2022, **5**, 9292–9296.
57 S. Hanabata, K. Kusada, T. Yamamoto, T. Toriyama, S. Matsumura, S. Kawaguchi, Y. Kubota, Y. Nishida, M. Haneda and H. Kitagawa, *J. Am. Chem. Soc.*, 2023, **146**, 181–186.
58 R. J. Spurling, E. A. Lass, X. Wang and K. Page, *Phys. Rev. Mater.*, 2022, **6**, 090301.
59 G. Du, C. Li, J. Li, G. Wu, Z. Huang, A. Mao, M. Ma, Z. Guo and Z. Chen, *J. Mater. Res. Technol.*, 2025, **35**, 265–288.
60 D. A. Vinnik, E. A. Trofimov, V. E. Zhivulin, S. A. Gudkova, O. V. Zaitseva, D. A. Zherebtsov, A. Y. Starikov, D. P. Sherstyuk, A. A. Amirov, A. V. Kalgin, S. V. Trukhanov and F. V. Podgornov, *Nanomaterials*, 2020, **10**, 268.
61 J. Liang, J. Liu, H. Wang, Z. Li, G. Cao, Z. Zeng, S. Liu, Y. Guo, M. Zeng and L. Fu, *J. Am. Chem. Soc.*, 2024, **146**, 7118–7123.
62 L. Zhou, D. Feng, Z. Li, H. Li, C. Ge, X. Zhang and T. Ma, *Adv. Funct. Mater.*, 2025, e14375.
63 A. H. Phakatkar, M. T. Saray, M. G. Rasul, L. V. Sorokina, T. G. Ritter, T. Shokuhfar and R. Shahbazian-Yassar, *Langmuir*, 2021, **37**, 9059–9068.
64 L. Luo, J. Ju, Y. Wu, X. Wan, W. Li, Y. Li, H. Jiang, Y. Hu and C. Li, *Adv. Mater.*, 2025, **37**, 2418856.
65 V. Strotkotter, O. A. Krysiak, J. Zhang, X. Wang, E. Suhr, W. Schuhmann and A. Ludwig, *Chem. Mater.*, 2022, **34**, 10291–10303.
66 Y. Yao, Z. Huang, T. Li, H. Wang, Y. Liu, H. S. Stein, Y. Mao, J. Gao, M. Jiao, Q. Dong, J. Dai, P. Xie, H. Xie, S. D. Lacey, I. Takeuchi, J. M. Gregoire, R. Jiang, C. Wang, A. D. Taylor, R. Shahbazian-Yassar and L. Hu, *Proc. Natl. Acad. Sci. U. S. A.*, 2020, **117**, 6316–6322.
67 Y. Yao, Q. Dong, A. Brozena, J. Luo, J. Miao, M. Chi, C. Wang, I. G. Kevrekidis, Z. J. Ren, J. Greeley, G. Wang, A. Anapolsky and L. Hu, *Science*, 2022, **376**, eabn3103.

68 H. Wu, Q. Lu, Y. Li, J. Wang, Y. Li, R. Jiang, J. Zhang, X. Zheng, X. Han, N. Zhao, J. Li, Y. Deng and W. Hu, *Nano Lett.*, 2022, **22**, 6492–6500.
69 J. Li, L. Luo, S. Wang, H. Song and B. Jiang, *PhotoMat*, 2024, 1–37.
70 J. Ahn, S. Park, D. Oh, Y. Lim, J. S. Nam, J. Kim, W. Jung and I. D. Kim, *ACS Nano*, 2023, **17**, 12188–12199.
71 V. D. Nguyen, T. Nagata and K. S. Chang, *Mater. Today Phys.*, 2023, **37**, 101202.
72 T. H. Piotrowiak, R. Zehl, E. Suhr, B. Kohnen, L. Banko and A. Ludwig, *Adv. Eng. Mater.*, 2023, **25**, 2300437.
73 G. Yin, H. Zhu, S. Chen, T. Li, C. Wu, S. Jia, J. Shang, Z. Ren, T. Ding and Y. Li, *Molecules*, 2025, **30**, 759.
74 L. Wu, T. Guo and T. Li, *iScience*, 2021, **24**, 102398.
75 D. Morgan, G. Pilania, A. Couet, B. P. Uberuaga, C. Sun and J. Li, *Curr. Opin. Solid State Mater. Sci.*, 2022, **26**, 100975.
76 J. G. Greener, S. M. Kandathil, L. Moffat and D. T. Jones, *Nat. Rev. Mol. Cell Biol.*, 2022, **23**, 40–55.
77 M. A. Buckingham, J. M. Skelton and D. J. Lewis, *Cryst. Growth Des.*, 2023, **23**, 6998–7009.
78 Y. Wang, J. Mi and Z.-S. Wu, *Chem. Catal.*, 2022, **2**, 1624–1656.
79 T. Afsharvosoughi and D. A. Crandles, *J. Appl. Phys.*, 2021, **130**, 184103.
80 H. X. Guo, W. M. Wang, C. Y. He, B. H. Liu, D. M. Yu, G. Liu and X. H. Gao, *ACS Appl. Mater. Interfaces*, 2022, **14**, 1950–1960.
81 M. Zhang, Y. Gao, C. Xie, X. Duan, X. Lu, K. Luo, J. Ye, X. Wang, X. Gao, Q. Niu, P. Zhang and S. Dai, *Nat. Commun.*, 2024, **15**, 8306.
82 D. Tatar, H. Ullah, M. Yadav, J. Kojcinovic, S. Saric, I. Szenti, T. Skalar, M. Finsgar, M. Tian, A. Kukovecz, Z. Konya, A. Sapi and I. Djerdj, *ACS Appl. Mater. Interfaces*, 2024, **16**, 29946–29962.
83 P. Ghigna, L. Airoldi, M. Fracchia, D. Callegari, U. Anselmi-Tamburini, P. D'Angelo, N. Pianta, R. Ruffo, G. Cibin, D. O. de Souza and E. Quartarone, *ACS Appl. Mater. Interfaces*, 2020, **12**, 50344–50354.
84 T.-Y. Chen, S.-Y. Wang, C.-H. Kuo, S.-C. Huang, M.-H. Lin, C.-H. Li, H.-Y. T. Chen, C.-C. Wang, Y.-F. Liao, C.-C. Lin, Y.-M. Chang, J.-W. Yeh, S.-J. Lin, T.-Y. Chen and H.-Y. Chen, *J. Mater. Chem. A*, 2020, **8**, 21756–21770.
85 A. Chroneos, *Appl. Sci.*, 2024, **14**, 5309.
86 S. Chae, L. Williams, J. Lee, J. T. Heron and E. Kioupakis, *npj Comput. Mater.*, 2022, **8**, 95.
87 V. A. Mints, K. L. Svane, J. Rossmeisl and M. Arenz, *ACS Catal.*, 2024, **14**, 6936–6944.
88 H. Cai, P. Zhang, B. Li, Y. Zhu, Z. Zhang and W. Guo, *Mater. Today Catal.*, 2024, **4**, 100039.
89 X. Duan, Y. Li, J. Zhao, M. Zhang, X. Wang, L. Zhang, X. Ma, Y. Qu and P. Zhang, *J. Am. Chem. Soc.*, 2025, **147**, 651–661.
90 X. Jia and H. Li, *J. Mater. Chem. A*, 2024, **12**, 12487–12500.
91 T. Cai, A. Chen, S. Liang, J. Mu, L. Wang, W. He, K. Tao, J. Li and F. Huang, *Adv. Mater.*, 2025, **37**, e08717.
92 J. T. Sivak, S. S. I. Almishal, M. K. Caucci, Y. Tan, D. Srikanth, J. Petruska, M. Furst, L. Q. Chen, C. M. Rost, J. P. Maria and S. B. Sinnott, *Phys. Rev. Lett.*, 2025, **134**, 216101.
93 S. H. Albedwawi, A. AlJaberi, G. N. Haidemenopoulos and K. Polychronopoulou, *Mater. Des.*, 2021, **202**, 109534.
94 S. Hou, X. Ma, Y. Shu, J. Bao, Q. Zhang, M. Chen, P. Zhang and S. Dai, *Nat. Commun.*, 2021, **12**, 5917.
95 J. Zhao, J. Bao, S. Yang, Q. Niu, R. Xie, Q. Zhang, M. Chen, P. Zhang and S. Dai, *ACS Catal.*, 2021, **11**, 12247–12257.
96 K. Mori, Y. Shimada, H. Yoshida, Y. Hinuma and H. Yamashita, *ACS Appl. Nano Mater.*, 2024, **7**, 28649–28658.
97 Y. Liao, Y. He, X. Cui and L. Liu, *Fuel*, 2024, **355**, 129494.
98 H. Chen, J. Fu, P. Zhang, H. Peng, C. W. Abney, K. Jie, X. Liu, M. Chi and S. Dai, *J. Mater. Chem. A*, 2018, **6**, 11129–11133.
99 C. Riley, A. De La Riva, J. E. Park, S. J. Percival, A. Benavidez, E. N. Coker, R. E. Aidun, E. A. Paisley, A. Datye and S. S. Chou, *ACS Appl. Mater. Interfaces*, 2021, **13**, 8120–8128.
100 H. Chen, K. Jie, C. J. Jafta, Z. Yang, S. Yao, M. Liu, Z. Zhang, J. Liu, M. Chi, J. Fu and S. Dai, *Appl. Catal., B*, 2020, **276**, 119155.
101 R. Li, Y. Ye, Y. Zhang, H. Zhao, W. Du and Z. Hou, *J. Mater. Chem. A*, 2024, **12**, 28753–28763.
102 Z. Yang, X. Xiang, J. Yang and Z.-Y. Zhao, *Mater. Futures*, 2024, **3**, 042103.
103 Q. Wang, X. Liu, D. He and D. Wang, *Mater. Today*, 2023, **70**, 218–236.
104 Z. Gao, D. Xiao, H. She, J. Zhong, X. Li, J. Huang, L. Wang and Q. Wang, *Nanoscale*, 2025, **17**, 23151–23161.
105 S. L. Fereja, Z. Zhang, Z. Fang, J. Guo, X. Zhang, K. Liu, Z. Li and W. Chen, *ACS Appl. Mater. Interfaces*, 2022, **14**, 38727–38738.
106 R. Liu, Y. Yan, L. Dun, T. Yang, B. Qin, P. Wang, W. Cai, S. Liu and X. Zheng, *Mater. Today Catal.*, 2025, **8**, 100086.
107 M. V. Kante, M. L. Weber, S. Ni, I. C. G. van den Bosch, E. van der Minne, L. Heymann, L. J. Falling, N. Gauquelin, M. Tsvetanova, D. M. Cunha, G. Koster, F. Gunkel, S. Nemsak, H. Hahn, L. Velasco Estrada and C. Baeumer, *ACS Nano*, 2023, **17**, 5329–5339.
108 Q. Zhang, Z. Zheng, R. Gao, X. Xiao, M. Jiao, B. Wang, G. Zhou and H. M. Cheng, *Adv. Mater.*, 2024, **36**, e2401018.
109 W. Li, Y. Wang, N. Xu and Y. Li, *J. Energy Storage*, 2025, **123**, 116784.
110 H. He, H. Yao, L. Sun, Y. Yang, Z. A. Qiao and B. Liu, *Adv. Mater.*, 2025, **37**, e08982.
111 O. Porodko, L. Kavan, M. Fabián, B. Pitňa Lásková, V. Šepelák, H. Kolev, K. L. da Silva, M. Lisnichuk and M. Zukalová, *Nanoscale*, 2025, **17**, 3739–3751.
112 Y. Zheng, X. Wu, X. Lan and R. Hu, *Processes*, 2021, **10**, 49.
113 L. Dong, Y. Tian, C. Luo, W. Zhao, C. Qin and Z. Wang, *Materials*, 2024, **17**, 1542.
114 H. K. Beere, N. S. Reddy, P. Kulkarni, K. Samanta, H. Y. Jung and D. Ghosh, *J. Energy Storage*, 2024, **80**, 110325.

115 C. Hong, R. Tao, S. Tan, L. A. Pressley, C. A. Bridges, H. Y. Li, X. Liu, H. Li, J. Li, H. Yuan, X. G. Sun and J. Liang, *Adv. Funct. Mater.*, 2024, **35**, 2412177.
116 X. Gao, X. Zhang, X. Liu, Y. Tian, Q. Cai, M. Jia and X. Yan, *Small Methods*, 2023, **7**, e2300152.
117 T. Cai, M. Cai, J. Mu, S. Zhao, H. Bi, W. Zhao, W. Dong and F. Huang, *Nano-Micro Lett.*, 2023, **16**, 10.
118 G. Caroline, N. Nair, S. V. Nair, P. Barpanda and S. Baskar, *Next Sustain.*, 2024, **4**, 100044.
119 Z. Wu, Q. Lv, W. Sun, H. Zhang, Y. Bai and C. M. Li, *J. Power Sources*, 2025, **634**, 236488.
120 K. Sun, J. Li, L. Li and D. Chao, *Chemistry*, 2025, **31**, e202402859.
121 S. Nundy, D. Tatar, J. Kojčinović, H. Ullah, A. Ghosh, T. K. Mallick, R. Meinusch, B. M. Smarsly, A. A. Tahir and I. Djerdj, *Adv. Sustainable Syst.*, 2022, **6**, 2200067.
122 S. Akrami, Y. Murakami, M. Watanabe, T. Ishihara, M. Arita, M. Fuji and K. Edalati, *Appl. Catal., B*, 2022, **303**, 120896.
123 P. Edalati, Q. Wang, H. Razavi-Khosroshahi, M. Fuji, T. Ishihara and K. Edalati, *J. Mater. Chem. A*, 2020, **8**, 3814–3821.
124 O. Guler, M. Boyrazli, M. G. Albayrak, S. H. Guler, T. Ishihara and K. Edalati, *Materials*, 2024, **17**, 853.
125 H. Ling, H. Sun, L. Lu, J. Zhang, L. Liao, J. Wang, X. Zhang, Y. Lan, R. Li, W. Lu, L. Cai, X. Bai and W. Wang, *Nat. Commun.*, 2024, **15**, 9505.
126 M. Anandkumar, A. Lathe, A. M. Palve and A. S. Deshpande, *J. Alloys Compd.*, 2021, **850**, 156716.
127 M. Anandkumar, P. K. Kannan, S. Sudarsan and E. A. Trofimov, *Surf. Interfaces*, 2024, **51**, 104815.
128 D. Jia, T. Chigan, X. Li, H. Li and P. Yang, *J. Alloys Compd.*, 2024, **982**, 173808.
129 N. Wen, X. Mu, Y. Zhu, Y. Huang, H. Chen, C. Han and L. Ye, *Langmuir*, 2024, **40**, 9020–9027.
130 S. Das, S. Kumar, S. Sarkar, D. Pradhan, C. S. Tiwary and S. Chowdhury, *J. Mater. Chem. A*, 2024, **12**, 16815–16830.